

1 **Co-variation of metabolic rates and cell-size in** 2 **coccolithophores**

3
4 **Giovanni Aloisi**

5
6 Laboratoire d'Océanographie et du Climat : Expérimentation et Approches Numériques

7 UMR 7159, CNRS-UPMC-IRD-MNHN, 75252 Paris, France

8 galod@locean-ipsl.upmc.fr; Tel +33 (0)1 44 27 70 72

9 10 11 **Abstract**

12 Coccolithophores are sensitive recorders of environmental change. The size of their
13 coccosphere varies in the ocean along gradients of environmental conditions and provides a
14 key for understanding the fate of this important phytoplankton group in the future ocean. But
15 interpreting field changes in coccosphere size in terms of laboratory observations is hard,
16 mainly because the marine signal reflects the response of multiple morphotypes to changes in
17 a combination of environmental variables. In this paper I examine the large corpus of
18 published laboratory experiments with coccolithophores looking for relations between
19 environmental conditions, metabolic rates and cell size (a proxy for coccosphere size). I show
20 that growth, photosynthesis, and to a lesser extent calcification, co-vary with cell size when
21 pCO₂, irradiance, temperature, nitrate, phosphate and iron conditions change. With the
22 exception of phosphate and temperature, a change from limiting to non-limiting conditions
23 always results in an increase in cell size. An increase in phosphate or temperature (below the
24 optimum temperature for growth) produces the opposite effect. The magnitude of the
25 coccosphere size changes observed in the laboratory is comparable to that observed in the
26 ocean. If the biological reasons behind the environment-metabolism-size link are understood,
27 it will be possible to use coccosphere size changes in the modern ocean and in marine
28 sediments to investigate the fate of coccolithophores in the future ocean. This reasoning can
29 be extended to the size of coccoliths if, as recent experiments are starting to show, coccolith
30 size reacts to environmental change proportionally to coccosphere size. The coccolithophore

31 database is strongly biased in favor of experiments with the coccolithophore *Emiliana*
32 *huxleyi* (*E. huxleyi*) (82% of database entries), and more experiments with other species are
33 needed to understand if these observations can be extended to coccolithophores in general. I
34 introduce a simple model that simulates the growth rate and the size of cells forced by nitrate
35 and phosphate concentrations. By considering a simple rule that allocates the energy flow
36 from nutrient acquisition to cell structure (biomass) and cell maturity (biological complexity,
37 eventually leading to cell division), the model is able to reproduce the co-variation of growth
38 rate and cell size observed in laboratory experiments with *E. huxleyi* when these nutrients
39 become limiting. These results support ongoing efforts to interpret coccosphere and coccolith
40 size measurements in the context of climate change.

41

42 **1 Introduction**

43 Coccolithophores, the main calcifying phytoplankton group, are an important component of
44 the oceanic carbon cycle (Broecker and Clark, 2009; Poulton et al., 2007). Through their
45 cellular processes of photosynthesis (a CO₂ sink) and calcification (a source of CO₂), they
46 contribute in defining the magnitude of the ocean-atmosphere CO₂ flux (Shutler et al., 2013).
47 The calcium carbonate platelets (coccoliths) that make up their exoskeleton (coccosphere)
48 provide ballast for dead organic matter in the photic zone, accelerating the export of carbon
49 from the upper ocean to the sediments (Honjo et al., 2008). There is laboratory and field
50 evidence that climate change is affecting the cellular processes and global distribution of
51 coccolithophores, with potential consequences on the magnitude of the carbon fluxes
52 introduced above (Gehlen, 2007; Wilson et al., 2012). For example, in laboratory cultures,
53 the coccolithophore *E. huxleyi* shows reduced calcification-to-photosynthesis ratios when
54 CO₂ is changed from pre-industrial levels to those predicted for the future, acidic ocean
55 (Hoppe et al., 2011; Langer et al., 2009; Riebesell et al., 2000; Zondervan et al., 2002). In the
56 ocean, the coccolithophore *E. huxleyi* has been expanding polewards in the past sixty years,
57 most likely driven by rising sea surface temperatures and the fertilizing effect of increased
58 CO₂ levels (Winter et al., 2013). Despite the great number of laboratory experiments testing
59 the effect of multiple environmental conditions on coccolithophore physiology (Iglesias-
60 Rodriguez et al., 2008; Langer et al., 2012; Paasche et al., 1996; Riebesell et al., 2000;
61 Riegman et al., 2000; Rouco et al., 2013; Sett et al., 2014; Zondervan, 2007; Zondervan et al.,

62 2002), it is hard to link laboratory results with field observations to obtain a unified picture of
63 how coccolithophores respond to changing environmental conditions (Poulton et al., 2014).

64 *E. huxleyi* is the most abundant, geographically distributed and studied coccolithophore
65 (Iglesias-Rodríguez, 2002; Paasche, 2001; Winter et al., 2013). It exhibits a strong genetic
66 diversity, with the different genotypes adapted to distinct environmental conditions (Cook et
67 al., 2011; Iglesias-Rodríguez et al., 2006; Medlin et al., 1996) – a characteristic that explains
68 its global distribution and ecological success in the modern ocean (Read et al., 2013). *E.*
69 *huxleyi* morphotypes, which differ for their coccosphere size, as well as shape, size and
70 degree of calcification of coccoliths (Young and Henriksen, 2003), correspond to at least
71 three genetically distinct genotypes (Cook et al., 2011; Schroeder et al., 2005). The
72 geographical distribution of *E. huxleyi* morphotypes in the ocean is controlled by
73 environmental conditions (Beaufort et al., 2008; Beaufort et al., 2011; Cubillos et al., 2007;
74 Henderiks et al., 2012; Poulton et al., 2011; Schiebel et al., 2011; Smith et al., 2012; Young
75 et al., 2014). But the physiological role of key factors such as pCO₂ is controversial, with a
76 study showing that high pCO₂ favors morphotypes with smaller and lighter coccoliths,
77 (Beaufort et al., 2011), and other studies showing the opposite (Grelaud et al., 2009; Iglesias-
78 Rodriguez et al., 2008; Smith et al., 2012). Next to pCO₂, there is growing evidence that
79 irradiance, nutrients and temperature also play a role in controlling morphotype biogeography
80 (Berger et al., 2014; Henderiks et al., 2012; Smith et al., 2012). Despite the need for a better
81 understanding, it is clear that the geographical distribution of *E. huxleyi* morphotypes carries
82 precious information on how this key coccolithophore species will react to climate change.

83 But there is another, more subtle effect of climate change on coccolithophores: as living
84 conditions evolve, cell-size and coccosphere-size adapt, due uniquely to a physiological
85 response to environmental change. At the cellular scale, laboratory experiments with *E.*
86 *huxleyi* show that pCO₂, irradiance, temperature and nutrient concentrations affect not only
87 rates of photosynthesis and calcification, but also cell and coccosphere size, without inducing
88 a change in morphotype (Bach et al., 2011; De Bodt et al., 2010; Iglesias-Rodríguez et al.,
89 2008; Muller et al., 2008; Müller et al., 2012; Oviedo et al., 2014; Rouco et al., 2013).
90 Culture conditions also affect the size and mass of coccoliths (Bach et al., 2012; Bollmann
91 and Herrle, 2007; Müller et al., 2012; Paasche et al., 1996; Satoh et al., 2008; Young and
92 Westbroek, 1991). Coccolith size (length, volume) and weight are used as proxies for
93 coccolithophore calcification because they are related to the total mass of calcite in the cell
94 (Beaufort et al., 2011) (although multiple layers of coccoliths around cells may complicate

95 this simple picture). The size of coccoliths is positively related to that of coccospheres in
96 laboratory experiments (Müller et al., 2012), in the ocean (Beaufort et al., 2008) and in
97 marine sediments (Henderiks, 2008), and the mass of coccoliths is positively related to that of
98 coccospheres in the ocean (Beaufort et al., 2011). These observations suggest that the
99 physiological sensitivity of coccosphere and coccolith size to environmental conditions
100 carries supplementary information on the reaction of *E. huxleyi* to climate change.

101 In the ocean, attempts are made to disentangle the effect of multiple environmental
102 parameters on the size and mass of *E. huxleyi* coccospheres and coccoliths (Beaufort et al.,
103 2008; Beaufort et al., 2011; Cubillos et al., 2007; Hagino et al., 2005; Henderiks et al., 2012;
104 Meier et al., 2014; Poulton et al., 2011; Young et al., 2014). This is a complicated task.
105 Primarily, as explained above, because changes in cell size are partly ecological in origin and
106 some automatic measuring procedures do not distinguish between the different morphotypes
107 (Beaufort et al., 2008; Beaufort et al., 2011; Meier et al., 2014). Second, because
108 environmental parameters co-vary in the field, making it hard to interpret size changes
109 observed in the ocean in terms of those recorded in the laboratory. Nevertheless, a recent
110 study based on scanning electron microscope observations suggests that the coccosphere size
111 of *E. huxleyi* within a population of a given morphotype varies considerably and is likely
112 under physiological control (Henderiks et al., 2012). Also the size of coccoliths of a given
113 morphotype varies in the modern ocean (Hagino et al., 2005; Henderiks et al., 2012; Poulton
114 et al., 2011) as well as the recent geological past (Berger et al., 2014; Horigome et al., 2014),
115 and is likely to be under the control of parameters other than pCO₂ (Horigome et al., 2014;
116 Young et al., 2014). To take advantage of the physiological and environmental information
117 carried by coccosphere and coccolith size, two steps need to be taken: first, the effect of
118 single environmental parameters on coccosphere and coccolith size has to be systematically
119 observed in the laboratory and, second, an understanding of the biological reasons behind
120 cell-size changes needs to be developed.

121 In this paper I explore the available laboratory data of coccolithophore metabolic rates and
122 cell-size. The metabolic rates considered are the growth rate (in units of day⁻¹), the rate of
123 photosynthesis (in units of pg_C cell⁻¹ day⁻¹) and the rate of calcification (in units of pg_C cell⁻¹
124 day⁻¹). First, I investigate how coccolithophore metabolic rates scale with cell-size in five
125 species of coccolithophores, and how this scaling compares to that of other phytoplankton
126 groups. Second, I discuss how metabolic rates and coccosphere size of a given
127 coccolithophore species are affected by changes in environmental culture conditions. The

128 laboratory changes in *E. huxleyi* coccosphere-size are compared to coccosphere size changes
129 observed in the modern ocean across gradients of environmental change. Finally, I propose a
130 simple model that explains why metabolic rates and cell-size co-vary, with the hope that a
131 few basic principles may be used in the future to extract environmental and metabolic
132 information from coccosphere and coccolith measurements obtained in the field. This paper
133 is based on a database of published results of culture experiments with coccolithophores - the
134 next section introduces this database.

135

136 **2 A database of coccolithophore metabolism and cell size**

137 The database (Table 1, appendix A1) is composed of data collected in 369 separate culture
138 experiments with 28 strains belonging to five species of coccolithophores (*E. huxleyi*,
139 *Gephyrocapsa oceanica*, *Calcidiscus leptoporus*, *Syracosphaera pulchra* and *Coccolithus*
140 *braarudii* (formerly known as *Coccolithus pelagicus*)). These studies were carried out in
141 batch reactors or chemostats, in a wide range of culture conditions, including variable
142 irradiance, light cycle, temperature, nutrient concentration (NO₃, PO₄ and Fe) calcium and
143 inorganic carbon concentrations (pCO₂, DIC, total alkalinity). The salinity and the
144 concentration of magnesium are similar to that of seawater. The database reports measured
145 values of growth rate μ , in units of day⁻¹, the organic (POC) and inorganic (PIC) carbon
146 quota, in units of pgC cell⁻¹, and the cell-specific rates of photosynthesis (RPh) and
147 calcification (RCa), in units of pgC cell⁻¹ day⁻¹. These quantities are interrelated according to
148 the following expressions:

$$149 \text{ RPh} = \mu \times \text{POC} \quad (1)$$

150 and

$$151 \text{ RCa} = \mu \times \text{PIC} \quad (2)$$

152 Equations 1 and 2 were used to complete the database when only two out of three of growth
153 rate, carbon content and cell-specific metabolic rates are presented in a given literature
154 source. When possible, the DIC system data has been converted to the total pH scale so that
155 pCO₂ can be compared across the dataset. The database includes 120 measurements of
156 coccosphere size carried out with coulter counters, flow cytometers and optical and scanning
157 electron (SEM) microscopes.

158 Some consideration of growth rate measurements in conditions of nutrient limitation is
159 necessary. In nutrient-limited batch cultures, the growth rate decreases in time as nutrients are
160 depleted, so that determining growth rates via cell counts yields erroneous results (Langer et
161 al., 2013). Reliable growth rates in conditions of nutrient limitation can be obtained in
162 chemostats, where the growth rate is controlled by setting the dilution rate of the medium and
163 the cell population is continuously renovated (Langer et al., 2013). An alternative are semi-
164 continuous cultures where cells are periodically harvested and inoculated into new medium,
165 allowing relatively constant growth conditions (LaRoche et al., 2010). When considering
166 nutrient limitation, I thus chosen to use only data produced in chemostat and semi-continuous
167 culture experiments.

168 **2.1 Normalized growth rates**

169 The light cycle varies from experiment to experiment, ranging from continuous light to a 12-
170 12h light-dark cycle. In order to compare the growth rates from experiments with different
171 light/dark cycles, the data needs to be normalized with respect to the duration of the light
172 period. Since photosynthesis is restricted to the light period, growth rates (μ , in day^{-1}) have
173 been normalized to the length of the light period. This is done applying the following
174 relationship (Rost et al., 2002):

$$175 \mu_i = \frac{\mu \times (L + D)}{L - D \times r} \quad (3)$$

176 where μ_i (in day^{-1}) is the normalized, instantaneous growth rate, μ (in day^{-1}) is the growth rate
177 measured via cell counts, L and D are the length (in hours) of the light and dark periods and r,
178 the factor which accounts for the respiratory loss of carbon during the dark period, is set to
179 0.15 (Laws and Bannister, 1980). Thus, the instantaneous growth rate μ_i , in units of day^{-1} , is
180 the growth rate normalized to a light period of 24 hrs.

181 **2.2 Normalized cell carbon quotas**

182 The organic carbon quota (POC) is positively related to cell volume. To compare POC across
183 the database, a large bias introduced by the sampling strategy needs to be considered.
184 Specifically, in experiments with a light/dark cycle, POC increases during the day as small
185 cells formed during nighttime division assimilate carbon and increase in size (Linschooten et
186 al., 1991; Muller et al., 2008; Vanbleijswijk et al., 1994; Zondervan et al., 2002). Typically,
187 sampling for POC measurements is carried out at different times during the light period in

188 different experiments. This introduces variability in the POC data that is not related to the
 189 experimental growth conditions. When the time of sampling in the light cycle is reported,
 190 POC data have been normalized with respect to the time of sampling using the following
 191 equation (the derivation of this equation is given in appendix A1):

$$192 \quad POC(t) = \frac{L \cdot POC(S_T)}{L + S_T} \cdot \left(1 + \frac{t}{L}\right) \quad (4)$$

193 where L is the length (in hours) of the light period, S_T is the sampling time in hours after the
 194 beginning of the light period, $POC(S_T)$ is the POC measured in the experiment at time S_T and
 195 t is the time at which the corrected POC value is calculated.

196 For experiments with a light/dark cycle where the sampling time is reported, I imposed $t =$
 197 $L/2$ in equation 4 to estimate the POC in the middle of the light phase. When the time of
 198 sampling is not reported, equation 4 was used to estimate a minimum and a maximum POC
 199 in the middle of the light phase assuming that the reported POC value was measured at the
 200 end and at the beginning of the light phase, respectively. This procedure was applied also to
 201 PIC values because inorganic carbon ($CaCO_3$) production takes place nearly exclusively
 202 during the light phase in coccolithophores (Muller et al., 2008) and PIC shows an evolution
 203 similar to POC during the light period (Zondervan et al., 2002). In experiments with
 204 continuous light the cell-cycle is desynchronized such that the average cell diameter remains
 205 constant if environmental conditions do not change (Muller et al., 2008; Müller et al., 2012).
 206 Thus, the POC measurements were not corrected in these experiments. Interestingly, fossil
 207 coccolithophores represent an integrated sample over the whole light:dark cycle and thus
 208 should be more comparable to laboratory samples from desynchronizes cultures – something
 209 to keep in mind as the amount of morphological data of coccolithophores from marine
 210 sediments is growing (Beaufort et al., 2011; Grelaud et al., 2009).

211 **2.3 Normalized cell-specific rates of photosynthesis and calcification**

212 The normalized growth rates and normalized cell carbon quota are used to calculate
 213 normalized, cell-specific rates of photosynthesis (RPh_i , in $pgC \text{ cell}^{-1} \text{ day}^{-1}$) and calcification
 214 (RCa_i , in $pgC \text{ cell}^{-1} \text{ day}^{-1}$):

$$215 \quad RPh_i = \mu_i \times POC_C \quad (5)$$

$$216 \quad RCa_i = \mu_i \times PIC_C \quad (6)$$

217 where the subscript C indicates that the carbon quota refers to the value in the middle of the
 218 light phase (calculated imposing $t = L/2$ in equation 4) and the subscript i indicates that the
 219 metabolic rates are normalized with respect to the light period (equation 3). Thus, RPh_i and
 220 RCa_i are the metabolic rates normalized to a light period of 24 hrs. When the time at which
 221 sampling occurred during the light period is not known, minimum and a maximum cell-
 222 specific rates of photosynthesis and calcification are calculated assuming that the reported
 223 POC and PIC values were measured at the end and at the beginning of the light phase,
 224 respectively.

225 **2.4 Estimating cell and coccosphere size from carbon quota**

226 Coccosphere size data is reported only in a third of the experiments included in the dataset
 227 (of which more than 80% of measurements are for *E. huxleyi*), while no cell-size
 228 measurements are included in the database. To take advantage of the full set of metabolic
 229 measurements available, cell-size and coccosphere size were estimated from the particulate
 230 organic (POC) and inorganic (PIC) carbon content per cell with the following expression (the
 231 full derivation is given in appendix A2):

$$232 \quad V_{Sphere} = \frac{1.8 \times POC}{d_{POM}} \cdot \left(1 + \frac{f_{CY}}{1 - f_{CY}}\right) + \frac{100}{12} \cdot \frac{PIC}{d_{CaCO_3}} \cdot \left(1 + \frac{f_{Sh}}{1 - f_{Sh}}\right) \quad (7)$$

233 where V_{Sphere} is the volume of the coccosphere (Fig. 1), the volume of the cell and shield are
 234 equal to the first and second term on the right in equation 7, respectively, d_{POM} (in $g\ cm^{-3}$) is
 235 the density of organic matter, d_{CaCO_3} (equal to $2.7\ g\ cm^{-3}$) is the density of $CaCO_3$ and f_{CY} and
 236 f_{Sh} are the volume fraction occupied by water in the cell and shield, respectively. Equation 7
 237 assumes that cell volume scales linearly with cellular carbon content. This assumption is
 238 reasonable for coccolithophores due to the absence of large vacuoles (Paasche, 1967).

239 I used equation 7 to calculate the diameter of the cell and the coccosphere for all the
 240 experiments in the database for which POC and PIC data are available (Fig. 2). The
 241 unknowns in this equation are d_{POM} , f_{CY} and f_{SH} . First, d_{POM} was set to $1.5\ g\ cm^{-3}$, which lies
 242 at the center of the range of values proposed by Walsby and Reynolds (1980) ($1.3 - 1.7\ g\ cm^{-3}$).
 243 Then f_{CY} and f_{SH} were varied so that the resulting diameter of the great majority of *E.*
 244 *huxleyi* spheres fell in the range $3 - 7.5\ \mu m$, which corresponds approximately to the range
 245 reported in culture experiments (Fig. 2) and to that measured microscopically in surface
 246 waters off the coast of the Benguela upwelling system (Henderiks et al., 2012). The chosen

247 values of f_{CY} (0.79) and f_{SH} (0.66) results in a difference between the diameter of the
248 coccosphere and that of the cell of about $1.5 \mu\text{m}$ for most of *E. huxleyi* the cells (values
249 significantly smaller or larger than $1.5 \mu\text{m}$ are interpreted in appendix A2). This value,
250 observed in cultures of *E. huxleyi* (Henderiks, pers. comm.), corresponds roughly to twice the
251 thickness of one layer of coccoliths (and thus to one layer of coccoliths in the shield around
252 one cell). This is consistent with the laboratory observation that in most calcifying *E. huxleyi*
253 cells regulate their calcification rates/division rates in order to maintain at least a complete
254 layer of coccoliths, even in growth-limited conditions (Paasche, 1999). With these parameter
255 settings, the resulting density of the naked *E. huxleyi* cell is $0.18 \text{ pgC } \mu\text{m}^{-3}$, which is
256 comparable to that of carbon in protist plankton of similar size determined by Menden-Deuer
257 and Lessard (2000). The cell diameter obtained with this procedure is compared with that
258 obtained applying an existing relation between POC and cell volume (Montagnes et al., 1994)
259 in appendix A1.

260 The calculated coccosphere diameter of *E. huxleyi* is compared to the measured coccosphere
261 diameter for the experiments in the database where POC, PIC and cell size data are reported
262 (Fig. 2b). Although a clear positive relation between measured and calculated coccosphere
263 size exists, the calculated diameters are always larger than the measured diameters (except
264 for two experiments in Kaffes et al. (2010)). The large majority of coccosphere size
265 measurements in the database were carried out with Coulter counters, which often do not
266 include the coccolith shield in the size measurement (Iglesias-Rodriguez et al., 2008; Oviedo
267 et al., 2014; van Rijssel and Gieskes, 2002). Consistently, the Coulter counter diameter for *E.*
268 *huxleyi* corresponds to the cell diameter calculated with equation 7 (Fig. 2b). Another source
269 for the observed discrepancy is the fact that in some experiments cells are fixed chemically
270 prior to size measurements, a treatment that induces cell shrinkage. Appendix A1 discusses
271 the discrepancy between measured and calculated coccosphere size more in detail. With these
272 consideration in mind, the choice made above of constraining equation 7 with the range of *E.*
273 *huxleyi* coccosphere diameters measured with the microscope (Henderiks, 2008) appears to
274 be the safest.

275 In figure 2c, the same parameterization of equation 7 is applied to the POC and PIC data
276 available for the other coccolithophore species. A comparison with published coccosphere
277 size data for some of these species suggests that approach is reasonable. Most of the
278 calculated coccosphere diameters for *Coccolithus braarudii*, for example, fall in the range

279 17-24 μm , which is slightly more extended than that reported by Henderiks (unpublished data
280 reported graphically in figure 7 of Henderiks (2008)) (18 – 22 μm). The corresponding shield
281 thickness for *Coccolithus braarudii* falls in two groups (4.5 μm and 7.5 μm) suggesting the
282 presence of more than one layer of coccoliths per cell in some cases. Similar to *E. huxleyi*,
283 the coccosphere diameter measured with Coulter counters is always smaller than the
284 calculated diameter (Fig. 2d). However, the discrepancy is small for these larger-sized
285 species. Significantly, the coccosphere diameter of *Calcidiscus leptoporus* measured with
286 SEM without prior fixing of cells by Langer et al. (2006) coincides with the calculated
287 coccosphere diameter using equation 7 (Fig. 2d). When discussing cell and coccosphere size
288 from experiments in the database I use equation 7 throughout the rest of this manuscript,
289 regardless if size measurements are reported in the literature sources or not.

290

291 **3 The allometric scaling of coccolithophore metabolism**

292 In this section the coccolithophore database is used to investigate relationships between cell
293 volume and metabolic rates across different taxa under comparable growth conditions
294 (allometric relations). The differences in metabolic rates we will deal with are largely due to
295 differences in characteristic cell size across different taxa. Allometric relationships for
296 coccolithophores will be compared with similar relations for other phytoplankton groups
297 compiled by Marañón (2008). The Marañón (2008) dataset includes cell volume and
298 metabolic rate data measured in the field for a vast array of unicellular photosynthetic
299 organisms spanning 9 orders of magnitude in size, from photosynthetic cyanobacteria
300 (volume = 0.1 μm^3) to large diatoms (volume = $10^8 \mu\text{m}^3$) and including dinoflagellates and
301 haptophytes. The Marañón (2008) dataset reports rate measurements that mostly reflect *in*
302 *situ* optimum growth conditions; thus, in this section, I focus on experiments in the
303 coccolithophore database that were carried out in optimum conditions (Table 2). The
304 assumptions made in comparing metabolic rates from the coccolithophore database with
305 those measured in the field by Marañón (2008) are detailed in appendix A2.

306 Figures 3a and 3b compare the allometric relations of photosynthesis and growth for
307 coccolithophores with those established by Marañón (2008) for phytoplankton. Figures 3c
308 and 3d show the allometric relations for photosynthesis and calcification in coccolithophores,

309 highlighting the position of the five different coccolithophore species considered. Linear
310 regressions through the optimum coccolithophore dataset yield the following equations:

$$311 \quad \text{Log}_{10}(\text{RPh}_i) = 0.89 \times \text{Log}_{10}(\text{Volume}) - 0.66 \quad (8)$$

$$312 \quad \text{Log}_{10}(\mu_i) = -0.11 \times \text{Log}_{10}(\text{Volume}) + 0.1 \quad (9)$$

$$313 \quad \text{Log}_{10}(\text{RCa}_i) = 1.02 \times \text{Log}_{10}(\text{Volume}) - 1.02 \quad (10)$$

314 The slope of the photosynthesis (0.89) and growth rate (-0.11) regressions for
315 coccolithophores is very similar to that of the Marañón (2008) dataset (0.91 and -0.09,
316 respectively) and comparable to the slope of the regression through the calcification rate data
317 (1.02). Furthermore, the different coccolithophore species occupy a position on the volume-
318 photosynthesis diagram that is dictated by their cell size (figure 3c). These plots show that,
319 for coccolithophores grown in optimum conditions, 1) photosynthesis in coccolithophores –
320 including five different species spanning nearly three orders of magnitude in cell size - scales
321 to cell volume in a comparable way as it does in other phytoplankton, 2) the size dependence
322 of growth rates is very small for coccolithophores, 3) calcification in optimum growth
323 conditions scales isometrically with cell volume.

324 The finding of a near-isometric scaling of coccolithophore growth in laboratory experiments
325 has implications for the scaling of phytoplankton population abundance with body size in the
326 ocean. In the ocean, including a variety of contrasting marine environments, phytoplankton
327 population abundance scales with body size with an exponent equal to $-3/4$: in other words,
328 small cells are more abundant than large cells (Cermeño et al., 2006). Reviews of laboratory
329 culture experiments with phytoplankton growth under optimal growth conditions suggest that
330 cell-specific photosynthesis rates scale with cell volume with an exponent of $3/4$ (Lopez-
331 Urrutia et al., 2006; Niklas and Enquist, 2001), possibly a consequence of the generic
332 properties of transportation networks inside the organisms (Banavar et al., 2002; West et al.,
333 1997). According to this scaling rule, growth rates scale with cell-size with an exponent of $-$
334 $1/4$, implying that large cells grow more slowly than small cells and offering an explanation
335 for the size scaling of population abundance with cell size observed in the field (Cermeño et
336 al., 2006).

337 However, the laboratory $-1/4$ scaling of growth rate to cell size has been challenged by the
338 observation that the same scaling in natural communities of phytoplankton is nearly isometric

339 (Huete-Ortega et al., 2012; Marañón, 2008; Marañón et al., 2007) (i.e. a slope in eq. 9 nearly
340 equal to 0 and no effect of cell size on growth rate). The size exponent for different
341 phytoplankton groups varies, with diatoms having a higher exponent (0.01) that of
342 dinoflagellates (-0.11) (Marañón, 2008) and whole community exponents varying from -0.01
343 (Marañón, 2008) to 0.16 (Huete-Ortega et al., 2012). An isometric scaling of growth rates to
344 cell volume has recently been also observed in laboratory experiments with 22 species of
345 phytoplankton ranging from 0.1 to $10^6 \mu\text{m}^3$ in volume (López-Sandoval et al., 2014; Marañón
346 et al., 2013). In this context the coccolithophore dataset is particularly relevant because it fills
347 in the gap of sizes between 10^0 and $10^3 \mu\text{m}^3$ that is underrepresented in Marañón's (2008)
348 dataset. Furthermore, it confirms that a scaling exponent significantly smaller than $-1/4$ occurs
349 in laboratory conditions, in addition to field situations, suggesting that cell-size is not an
350 important factor in determining the size distribution of coccolithophore populations. Taken
351 together, the near-isometric scaling of growth rate with cell size observed in the ocean by
352 Marañón (2008) and in the laboratory (López-Sandoval et al., 2014; Marañón et al., 2013)
353 suggest that the $-3/4$ scaling of phytoplankton population abundance with cell size is not due
354 uniquely to an effect of cell size on growth rates.

355 We are left with a contradiction that needs to be explained: whereas in some cases growth
356 rates in the laboratory scale with cell-size with an exponent of $-1/4$ (Lopez-Urrutia, 2006;
357 Niklas and Enquist, 2001), this is not the case in the ocean (Huete-Ortega et al., 2012;
358 Marañón, 2008; Marañón et al., 2007) and in some laboratory experiments (López-Sandoval
359 et al., 2014; Marañón et al., 2013). With regard to laboratory experiments, López-Sandoval et
360 al. (2014) point out that this difference could be in part due to the fact that older compilations
361 of experimental data do not include cells smaller than $100 \mu\text{m}^3$. In the ocean, the larger
362 phytoplankton (e.g. diatoms) have the ability to move vertically in the water column and
363 adapt to variable nutrient and light conditions (Mitrovic et al., 2005; Stolte et al., 1994). This
364 confers an advantage over small phytoplankton cells and provides a possible explanation for
365 the near-isometric scaling of natural phytoplankton communities (Marañón, 2008). In
366 laboratory experiments, where environmental parameters are typically constant, such
367 extrinsic factors cannot be at play and some intrinsic, cellular-level, property of
368 coccolithophore cells must exist that allows larger coccolithophores to overcome the
369 geometrical constraints imposed by cell size on resource acquisition (Raven, 1998). Some
370 coccolithophores possess carbon concentrating mechanisms (CCMs) that enable cells to take
371 up HCO_3^- , as well as CO_2 , for photosynthesis, and interconvert HCO_3^- to CO_2 internally via

372 the carbonic anhydrase enzyme (Reinfelder, 2011; Rost et al., 2003). There is evidence from
373 the carbon stable isotope composition of coccolithophore calcite that large coccolithophore
374 species employ CCMs more efficiently than small species when CO₂ is scarce (Bolton and
375 Stoll, 2013). This differential use of CCMs in large and small coccolithophore species offers
376 a plausible (even if not exclusive) explanation of why coccolithophore growth rate scales
377 nearly isometrically with cell size in laboratory experiments.

378

379 **4 Environmental controls on cell size and metabolic rates in** 380 **coccolithophores**

381 In this section I investigate how changes in environmental conditions affect cell size and
382 metabolic rates in coccolithophores. The changes we will deal with are produced by the
383 physiological response of a given taxon to environmental change; I will discuss the effects of
384 six environmental variables: pCO₂, irradiance, temperature, nitrate, phosphate and iron. Next
385 to the optimum group of experiments introduced in section 3, I highlight light-limited,
386 nitrate-limited, phosphate-limited and iron-limited experiments. The set of conditions
387 defining these groups is detailed in table 2. Most of the data (82 % of database entries) comes
388 from cultures of *E. huxleyi*, the more thoroughly studied coccolithophore; experiments with
389 the other four coccolithophores in the database have essentially tested the effect of pCO₂
390 conditions on growth, photosynthesis and calcification.

391 Within the optimum group of experiments, the position of the high-CO₂ subgroup largely
392 corresponds to that of the low pCO₂ group (Fig. 4). A considerable number of data points
393 collected in sub-optimal growth conditions, however, fall below the regression line through
394 the optimal data. The scatter is greater for *E. huxleyi* reflecting the fact that a much smaller
395 number of environmental conditions have been tried out for the other species. For all rates of
396 growth, photosynthesis and calcification, the light-limited experiments consistently plot
397 below the optimum experiments (Fig. 4). The position of the nutrient-limited experiments
398 below the optimum experiments is even more evident (Fig. 4): light-limited and nutrient
399 limited cells have smaller metabolic rates than cells of comparable size grown in optimum
400 conditions. For experiments where the sampling time during the light period is unknown, the
401 range of values for the photosynthetic rate (error bars) is large and an overlap with optimum
402 group of experiment exists. However, only 5 out of 30 experiments in the light-limited group
403 and 9 out of 31 nutrient-limited experiments have unknown sampling times, such that the

404 position of the experiments run in limiting conditions under the optimum group of
405 experiments is significant.

406 The plots of volume against metabolic rates introduced above do not take advantage of the
407 whole potential of the experimental dataset. This is because part of the variability in
408 metabolic rates observed is due to differences in the pre-culture conditions and, very likely,
409 to biological variability, rather than to the experimental conditions that the experiments are
410 designed to test. A better picture is obtained if *changes* in cell volume are plotted against
411 *changes* in metabolic rates. I have explored the database for sets of experiments where only
412 one experimental condition is changed at a time, so that the change in volume and metabolic
413 rates can be calculated by subtraction and plotted. In this way different sets of experiments
414 can be compared on the same plot (this procedure is explained in detail in appendix A3). The
415 plots show the changes in metabolic rates and cell size induced by an increase in pCO₂, an
416 increase in irradiance starting from light-limited conditions, an increase in temperature and a
417 decrease in nitrate, phosphate or iron starting from nutrient-replete conditions (figures 5 and
418 6). These changes correspond to the evolution of the living conditions that phytoplankton are
419 experiencing (warming, acidification) or are planned to experience (ocean stratification
420 leading to increased irradiance and oligotrophy) in the coming centuries (Behrenfeld et al.,
421 2006; Bopp, 2005; Bopp et al., 2001). Tables 3 and 4 summarize the changes in cell and
422 coccosphere diameter and volume induced by changes in experimental culture conditions.
423 They highlight an important fact: changes in pCO₂ produce only limited variations in
424 coccosphere size compared to variations in other parameters such as irradiance, temperature
425 and nutrients.

426 **4.1 pCO₂ increase**

427 For the low-pCO₂ group of experiments run in optimum conditions (Fig. 5), an increase in
428 pCO₂ leads to an increase in cell size and little change in the growth rate. The rate of
429 photosynthesis increases with pCO₂, indicating that *E. huxleyi* is carbon-limited in this range
430 of pCO₂. The biomass-specific calcification rate decreases in the great majority of the
431 experiments, while the change in the rate of calcification can be positive or negative.
432 Interestingly, the response of photosynthesis and calcification differ not only in sign, but also
433 in homogeneity: while the change in photosynthetic rate defines a clear trend in the volume-
434 metabolism space, the change in calcification rate is poorly correlated with the change in cell
435 volume. This is not surprising given that the rate of photosynthesis increases both due to the

436 fertilizing effect of CO₂ (physiological effect) and due to the increase in cell size (geometric
437 effect), while the rate of calcification is positively affected by the increase in cell-size
438 (geometric effect) but inhibited physiologically by acidification (Raven and Crawford, 2012).
439 This complex reaction of calcification to changes in the DIC system has been elegantly
440 captured in a recent model equation developed by (Bach et al., 2015). Furthermore, the
441 response of calcification to a rise in pCO₂ is modulated by the growth temperature (which
442 varies between experiments) and can be negative or positive (Sett et al., 2014). Finally, the
443 response of calcification in *E. huxleyi* to an increase in pCO₂ is known to be strain-specific,
444 with a large span of responses possible (Langer et al., 2006). In all experiments but 3, the
445 ratio of calcification to photosynthesis decreases following the pCO₂ increase. Overall, the
446 changes observed for the low pCO₂ group of optimum experiments occur also in the high-
447 pCO₂ group of experiments (albeit with a larger scatter) and in the experiments run in
448 conditions of light limitation (Fig. 5). The few experiments available where pCO₂ is varied in
449 conditions of nitrate limitation seem to point to a similar behavior (see appendix A3), as do
450 the data available for other coccolithophore species (Fig. 5).

451 **4.2 Irradiance increase in light-limited conditions**

452 Increasing irradiance from irradiance-limited conditions leads to a large increase in cell-size,
453 growth rate and rate of photosynthesis (Fig. 6). In the majority of experiments also the
454 biomass-specific and cell-specific rate of calcification increase with irradiance. The effects
455 on the calcification-to-photosynthesis ratio are large, with most experiments showing an
456 increase in calcification compared to photosynthesis. These effects are observed both in low
457 pCO₂ and in high-pCO₂ conditions; they can be understood considering that both
458 photosynthesis and calcification are light-dependent, energy-requiring processes (Brownlee et
459 al., 1995; Raven and Crawford, 2012). Interestingly, there is a smaller dispersion in the
460 calcification rate data compared to the set of experiments where pCO₂ is increased (figure 5).
461 This is because both the geometric and physiological consequences of an irradiance increase
462 concur in increasing the rate of calcification (geometric and physiological effects have
463 contrasting influence on calcification rate for a pCO₂ rise). The experiments showing a
464 negative response of the PIC/POC ratio with increased irradiance are from Rokitta and Rost
465 (2012) and Feng et al. (2008) where high light intensities were used (300 and 400 μmol m⁻²
466 s⁻¹, respectively), possibly inducing photoinhibition of calcification (Feng et al., 2008).

467 **4.3 Temperature**

468 Both in optimum and in light-limited conditions, an increase in temperature leads to an
469 increase in the growth, photosynthesis and calcification rate and a decrease in cell size in the
470 majority of the experiments considered (the scatter is considerable). This is consistent with
471 the observation that *E. huxleyi* has highest growth rate at temperatures 5-10°C higher than the
472 maxima observed at the isolation sites (Sett et al., 2014) – a pattern that seems to apply in
473 general to phytoplankton from polar and temperate regions (Atkinson et al., 2003; Thomas et
474 al., 2012). This trend has also been described in an long-term experiment during which *E.*
475 *huxleyi* was allowed to adapt for 1 year (roughly 460 asexual generations) to high
476 temperatures (Schlüter et al., 2014).

477 **4.4 NO₃, PO₄ and Fe limitation**

478 Under nitrogen limitation all cell-specific and biomass-specific metabolic rates decrease and
479 cells become smaller (Fig. 6). The same effect on metabolic rates is observed under
480 phosphorous limitation, but the effect on cell size is opposite (Fig. 6). The contrasting effect
481 of nitrogen and phosphorous limitation on cell size depends on the different role of these
482 nutrient in the cell cycle (Muller et al., 2008). In the G1 (assimilation) phase of the cell-cycle,
483 nitrogen consumption by *E. huxleyi* cells is high because cells are synthesizing and
484 accumulating biomass (Muller et al., 2008). Therefore, nitrogen depletion decreases
485 assimilation rates and leads to smaller cells. The result is not dissimilar from what happens
486 during light limitation. Phosphorous consumption, instead, is highest during the S and G2 +
487 M phases, due to synthesis of nucleic acids and membrane phospholipids immediately before
488 cell division (Geider and La Roche, 2002; Muller et al., 2008). Thus, phosphorous limitation
489 is though to arrest the cells in the G1 (assimilation) phase of the cell cycle, increasing the
490 length of this phase and leading to an increase in the cell-size. Thus, in phosphorous limited
491 cells, cell-size does not increase because the assimilation rate increases but because the
492 assimilation period is longer. The change in the ratio of photosynthesis to calcification is
493 generally positive. In the only set of experiments considering iron limitation (Schulz et al.,
494 2007), cell-size co-varies with growth and photosynthesis rates in a similar way as in nitrate-
495 limited experiments (Fig. 6). Iron is a key component of carbon concentrating mechanisms
496 (CCMs) that increase the rate of import of inorganic carbon (CO₂ and HCO₃⁻) for
497 photosynthesis, and of chlorophyll; thus, under iron-limiting conditions, the decrease in
498 metabolic rates is produced by carbon-limitation (Schulz et al., 2007). The concomitant
499 decrease in cell-size is consistent with the size shifts observed in the experiments where
500 pCO₂ is varied (Fig. 5).

501 It should be noted that the coccolithophore database is strongly biased in favor of
502 experiments with the coccolithophore *E. huxleyi* (82% of database entries), and more
503 experiments with other species are needed to understand if the above relations between
504 environment, cell size and metabolic rates can be extended to coccolithophores in general.
505 Furthermore, the experiments included in the coccolithophore dataset are designed to
506 quantify the instantaneous (meaning a few generations) response of coccolithophores to
507 changing growth conditions. In longer-term experiments, lasting several hundred generations,
508 (Lohbeck et al., 2012; Schlüter et al., 2014) *E. huxleyi* has been observed to adapt to elevated
509 temperatures and pCO₂ conditions simulating future ocean conditions. This implies that the
510 trends of metabolic rates and cell-size with changing environmental conditions that are
511 described in this section will be modulated by evolutionary adaptation, adding further
512 complexity to the interpretation of past and future response of coccolithophores to climate
513 change. The results of these experiments show, however, that the long-term response of
514 growth rate and cell size to increased temperature and increased pCO₂ are qualitatively
515 comparable: cells adapted to high temperature decrease their cell-size while cells adapted to
516 high pCO₂ increase their cell size (Schlüter et al., 2014).

517

518 **5 The size of *E. huxleyi* in the ocean: is there hope of detecting a** 519 **physiological signal ?**

520 In the previous section we saw that a change in laboratory culture conditions nearly always
521 results in a change of cell and coccosphere-size of coccolithophores. In this section the
522 changes in coccosphere size observed in laboratory experiments are compared to those
523 observed in the ocean. I will consider in some detail the BIOSOPE transect that crosses the
524 south pacific gyre from the Marqueses islands to the Peru upwelling zone (Beaufort et al.,
525 2008). Figure 7a shows the BIOSOPE transect superimposed on a surface ocean chlorophyll
526 concentraion map obtained from satellite observations. Figure 7b is a vertical transect in the
527 upper 300 m of the ocean showing the variability of the diameter of coccospheres belonging
528 to the order Isochrysidales. The order Isochrysidales is composed of the genera *Emiliana*,
529 *Geophyrocapsa* and *Crenalithus*. These genera cannot be distinguished from one another by
530 the automated SYRACO system used to measure coccosphere diameter and generate figure
531 7b. In addition to SYRACO, the BIOSOPE samples were examined with a Scanning Electron

532 Microscope and a light microscope which process less samples than SYRACO but are able to
533 distinguish the different Isochrysidales genera.

534 Along the BIOSOPE transect the diameter and volume of Isochrysidales coccospheres
535 measured with SYRACO varies considerably (from 4.5 to 8 μm figure 7b). Scanning
536 Electron Microscope and light microscope observations show that between 140°W and
537 130°W, where coccospheres are largest (mostly > 6 μm in diameter), *Gephyrocapsa oceanica*
538 dominates the Isochrysidales assemblage (Beaufort et al., 2008). *Gephyrocapsa oceanica* has
539 a characteristic cell size which is slightly larger than *E. huxleyi* (figure 3). In the Peru
540 upwelling zone (75°W) where SYRACO detects large coccospheres (mostly > 6 μm in
541 diameter), microscope observations show that *E. huxleyi* morphotype R, which is
542 characteristically large (“over-calcified”), is abundant. Clearly, changes in coccosphere size
543 along the BIOSOPE transect are partly ecological in origin – an observation that can be
544 exported to the global ocean (Beaufort et al., 2011).

545 But how do the cell-size changes observed along the BIOSOPE transect compare with those
546 observed in laboratory experiments? Whereas in the ocean changes in cell size can be due to
547 both ecological and physiological effects, in the laboratory only physiological effects are
548 expected. The histograms of figure 8a and 8b show the coccosphere diameter and volume of
549 cultured *E. huxleyi* cells and of the *Isochrysidales* coccolithophores in the BIOSOPE transect.
550 Laboratory and field measurements compare well. The red horizontal bar graphs of figures 8a
551 and 8b are the changes in coccosphere diameter and coccosphere volume observed in
552 laboratory experiments for given variations in culture conditions (see also Tables 3 and 4).
553 The comparison of histograms and bar charts shows that the variability of cell-size in
554 laboratory cultures is similar to that observed in the BIOSOPE transect. In figure 8c, the
555 range of environmental conditions imposed in laboratory cultures are compared with the
556 range of environmental conditions along the BIOSOPE transect. Large differences in the total
557 range exist only for phosphate and iron, with concentrations in limited experiments being
558 much lower than those measured in the BIOSOPE transect. Even discarding the phosphate
559 and iron limitation experiments, it is clear that changes in environmental conditions along the
560 BIOSOPE transect are very likely to be an important driver of coccosphere size variability:
561 *physiological* effects concur with *ecological* effects in determining coccolithophore cell-size
562 variability.

563 Further evidence for a physiological control on coccosphere size in the ocean comes from the
564 Benguela coastal upwelling system, where the size of the well-calcified *E. huxleyi*
565 morphotype A* (determined by SEM observations) changes considerably with environmental
566 conditions (Henderiks et al., 2012). The largest coccospheres occurred at the depth of the
567 deep chlorophyll maximum (DCM) – where growth conditions can be assumed to have been
568 more favorable than in the overlying and underlying water masses - whereas coccospheres
569 above and below the DCM were significantly smaller. This is consistent with the laboratory
570 observations (section 4) that environmental conditions which result in large growth rates (and
571 thus lead to large populations in the field) are also those that give rise to large cells
572 (phosphate concentrations in the Benguela upwelling system were much larger than those
573 which induce an increase in cell size in culture experiments).

574 Another, even less explored (but equally promising), avenue of research is that of the
575 physiological control of environmental conditions on the size of coccoliths. Field
576 measurements of coccolith size are more abundant than measurements of coccosphere size.
577 However, as for coccospheres, it is difficult to disentangle physiological from ecological
578 effects. Clearly, different morphotypes occupy distinct ecological niches characterized by
579 different environmental conditions. For example, Cubillos et al. (2007) show that Type A
580 (“overcalcified”) and Type B/C morphotypes occupy distinct latitudinal zones in the southern
581 ocean. Environmental conditions likely control the geographical distribution of different
582 morphotypes on the east coast of Japan (Hagino et al., 2005), the Bay of Biscay (Smith et al.,
583 2012), the Patagonian shelf (Poulton et al., 2011) and the South East Pacific (Beaufort et al.,
584 2008). Clearly, part of the variability in coccolith size distribution in the global ocean is due
585 to ecological effects (Beaufort et al., 2011).

586 There is laboratory and field evidence, however, that coccolith size is affected by
587 environmental conditions also via physiological effects. Coccosphere and coccolith size are
588 related (Henderiks, 2008). In laboratory cultures subject to varying pCO₂ and nitrate levels,
589 coccolith volume (which is related to coccolith length) is positively correlated to both cell
590 and coccosphere size (Müller et al., 2012), leading to the counterintuitive co-existence of
591 large coccoliths and acidic conditions. An increase in the size of coccoliths with increasing
592 pCO₂ has also been observed in nutrient replete, nitrogen-limited and phosphate-limited
593 experiments (Rouco et al., 2013). In the Benguela coastal upwelling system a significant
594 positive correlation has been found between the coccosphere diameter and coccolith length of
595 *E. huxleyi* morphotype A* (Henderiks et al., 2012). Since the Benguela correlation is based

596 on SEM observaions, it is likely that ecological effects can be excluded and that the
597 physiological effects that produce larger coccospheres also result in the production of larger
598 coccoliths. More in general, when the coccolith size from individual morphotypes is
599 measured along gradients of environmental conditions, it results that coccolith size varies
600 significantly; for example off the eastern coast of Japan (Hagino et al., 2005) and along the
601 Patagonian shelf (Poulton et al., 2011). More experiments and field observations are needed
602 to understand how other environmental parameters (e.g. temperature, irradiance and nutrient
603 availability) affect coccolith size, and to what extent laboratory observations can be exported
604 to the ocean. The available information suggests, however, that the environment controls
605 coccolith size via a physiological effect and that there could be as much hidden information
606 in the size of coccoliths as there is in the size of coccospheres - in the next section I propose a
607 way to extract this information from the modern ocean and sedimentary record.

608

609 **6 A theoretical basis for interpreting the co-variation of metabolic rates and** 610 **cell size**

611 We saw that metabolic rates and cell-size co-vary in coccolithophores subject to changes in
612 laboratory environmental conditions (section 4) and that the changes in coccosphere size
613 observed in the laboratory are comparable in magnitude to those observed in the field along
614 gradients of environmental change (section 5). If the cellular processes that give rise to this
615 co-variation are understood, there is hope that coccosphere-size measurements from the field
616 will yield information on the metabolic status of cells in the modern ocean and, possibly, on
617 past environmental conditions. In this section I introduce a simple model that provides a
618 theoretical basis for understanding how cellular metabolism - forced by environmental
619 conditions - controls cell-size, giving rise to the correlations described in section 4.

620 The mean size of dividing cells is the result of two factors: the rate of nutrient assimilation
621 into biomass and the length of the generation time (the time between two successive cell
622 divisions) - long generation times and large rates of nutrient assimilation give rise to large
623 cells, and vice versa. The changes in cell size observed in the previous section can be
624 interpreted within this simple scheme. The central concept I use – that of separation of
625 *structure* (biomass) from *maturity* (biological complexity, eventually leading to cell division)
626 - is taken from the Dynamic Energy Budget (DEB) Theory (Kooijman, 2010). The model
627 presented here is much simplified compared to existing DEB models of phytoplankton cells

628 (Lorena et al., 2010; Muller et al., 2011; Muller and Nisbet, 2014). However, it considers the
 629 minimum number of concepts that are necessary to explain the co-variance of metabolic rates
 630 and cell-size we are dealing with. The most important simplifications I introduce are
 631 discussed in appendix A4; the mathematical notation in this section follows that of
 632 (Kooijman, 2010).

633 Consider a spherical growing cell assimilating NO₃ and PO₄ (CO₂ is considered to be non-
 634 limiting). The assimilation rate of nutrients, \dot{J}_i (in $\mu\text{mol cell}^{-1} \text{day}^{-1}$), is proportional to the
 635 surface of the cell (Figure 9):

$$636 \quad \dot{J}_i = S \cdot j_{i\max} \cdot \frac{[i]}{[i] + K_i} \quad (11)$$

637 where the subscript i represents either NO₃ or PO₄, $j_{i\max}$ (in $\mu\text{mol } \mu\text{m}^{-2} \text{day}^{-1}$) is the surface-
 638 specific maximum nutrient uptake rate, S (in $\mu\text{mol } \mu\text{m}^{-2}$) is cell surface, K_i (mol litre⁻¹) is a
 639 Monod constant for nutrient uptake and $[i]$ (in mol litre⁻¹) is the nutrient concentration. Both
 640 the cell surface and the rate of nutrient assimilation are time dependent because the model
 641 simulates a growing cell. Values of $j_{i\max}$ were set equal to 4×10^{-9} and values of K_i were set
 642 equal to $0.2 \mu\text{mol litre}^{-1}$ and $2 \text{ nmol litre}^{-1}$ for NO₃ and PO₄, respectively, which is in the
 643 range of values determined for *E. huxleyi* (Riegman et al., 2000).

644 Assimilated nutrients are used to undertake two fundamental tasks (figure 9): 1) increase the
 645 cellular biomass via production of *structure* and 2) increase the *maturity* of the organism. In
 646 DEB theory the *structure* (quantified in moles of carbon per cell) contributes to the biomass
 647 of the organism (and thus cell volume) and is composed of organic compounds that have a
 648 long residence time in the cell. *Maturity* (quantified in Joules per cell) has the formal status of
 649 information and is a measure of the complexity of the organism (Kooijman, 2010).

650 Fundamental biological events in the lifespan of an organism, such as cell division, take place
 651 at a threshold level of *maturity*. Assimilated N and P both contribute to structure and maturity
 652 via the fluxes \dot{J}_{G_i} and \dot{J}_{MAT_i} such that mass is conserved:

$$654 \quad \dot{J}_{G_i} = \kappa \cdot \dot{J}_i \quad (12)$$

655 and

656 $\dot{J}_{MAT_i} = (1 - \kappa) \cdot \dot{J}_i$ (13)

657 where κ , which takes a value from 0 to 1, is the portion of the nutrient uptake flux which is
 658 dedicated to growth, and \dot{J}_{G_i} and \dot{J}_{MAT_i} (in $\mu\text{mol}_i \text{ cell}^{-1} \text{ day}^{-1}$) are the fluxes dedicated to
 659 growth and maturity, respectively. Dimensionless parameter κ was set equal to 0.5 both for
 660 NO_3 and for PO_4 .

661 The growth fluxes generated from nutrient uptake, \dot{J}_{G_i} , are sent to a synthesizing unit (SU)
 662 for growth where biomass is synthesized at a rate \dot{J}_G (in $\text{mol}_C \text{ cell}^{-1} \text{ day}^{-1}$):

663

664
$$\dot{J}_G = 10^{-6} \cdot CN_{BIO} \cdot \left[\sum_{i=N,P} \left(\frac{\dot{J}_{G_i}}{y_{G_i}} \right)^{-1} - \left(\sum_{i=N,P} \frac{\dot{J}_{G_i}}{y_{G_i}} \right)^{-1} \right]^{-1}$$
 (14)

665

666 where CN_{BIO} is the Redfield C/N ratio (equal to 106/16), necessary to transform the growth
 667 rate from units of $\text{mol}_N \text{ cell}^{-1} \text{ day}^{-1}$ to $\text{mol}_C \text{ cell}^{-1} \text{ day}^{-1}$, and parameters y_{G_i} are the yield of
 668 nutrient flux i to the structure. The maturation fluxes generated from nutrient uptake, \dot{J}_{MAT_i} ,
 669 are sent to another SU which tracks the build up of maturity in the cell with a rate \dot{p}_R (in
 670 $\text{Joules cell}^{-1} \text{ day}^{-1}$):

671

672
$$\dot{p}_R = 10^{-6} \cdot CN_{BIO} \cdot \mu_{MAT} \cdot \left[\sum_{i=N,P} \left(\frac{\dot{J}_{MAT_i}}{y_{MAT_i}} \right)^{-1} - \left(\sum_{i=N,P} \frac{\dot{J}_{MAT_i}}{y_{MAT_i}} \right)^{-1} \right]^{-1}$$
 (15)

673

674 where μ_{MAT} (in Joules mol_C^{-1}) is the chemical potential of maturity (set equal to 10^5 joules
 675 mol_C^{-1}) and the parameters y_{MAT_i} are the yield of nutrient flux i to maturity. In this simple
 676 model, I set the yield parameters in equations x and y such that NO_3 contributes primarily to
 677 the structure ($y_{G_{NO_3}} = 1$; $y_{G_{PO_4}} = 0.6$) and PO_4 to maturity ($y_{MAT_{NO_3}} = 0.6$; $y_{MAT_{PO_4}} = 1$).

678 The build-up of structure M_V (in $\text{mol}_C \text{ cell}^{-1}$) and maturity E_H (in Joules cell^{-1}) is tracked by
 679 the following differential equations:

680

$$681 \quad \frac{dM_V}{dt} = J_G \quad (16)$$

$$682 \quad \frac{dE_H}{dt} = P_R \quad (17)$$

683

684 in DEB theory volume, V (in μm^3), is obtained from the structural mass (the maturation flux
 685 is considered to dissipate in the environment and thus does not contribute to cell volume):

$$686 \quad V = \frac{M_V \cdot \mu_V}{[E_G]} \quad (18)$$

687 where μ_V (Joules mol_C^{-1}) is the chemical potential of the structure and $[E_G]$ (in $\text{Joules } \mu\text{m}^{-3}$)
 688 represents the volume-specific growth costs. In equation 18, the ratio of the chemical
 689 potential of the structure to the volume-specific growth costs can be obtained from the
 690 density of carbon in biomass, C_{BIO} , which is equal to $0.18 \text{ pg}_C \mu\text{m}^{-3}$ for *E. huxleyi* (section
 691 3):

$$692 \quad \frac{\mu_V}{[E_G]} = 10^{12} \cdot \frac{m_C}{C_{BIO}} \quad (19)$$

693 where m_C (=12) is the molecular weight of carbon and the factor 10^{12} is needed to convert
 694 pg_C to g_C . Thus, substituting the right hand side of equation 19 in equation 18, the model
 695 calculates cell volume as follows:

$$696 \quad V = \frac{M_V \cdot m_C \cdot 10^{12}}{C_{BIO}} \quad (20)$$

697 At any time, the instantaneous growth rate μ_{INST} (in day^{-1}) can be calculated as the ratio of the
 698 carbon uptake rate and the cellular carbon quota:

$$699 \quad \mu_{INST} = \frac{J_G}{M_V} \quad (21)$$

700 Figure 10 shows how maturity, cell volume and the instantaneous growth rate (calculated
701 with equation 21) evolve during a typical model run in non-limiting conditions. The model is
702 run starting with initial cell size equal to $10 \mu\text{m}^3$. As nutrients are taken up, they contribute to
703 the structure. Biomass and cell size increase. As the cell grows maturity accumulates, until
704 the threshold maturity for cell division is attained (dashed red line in figure 10a). The cell
705 divides and a new cell cycle starts. After cell division the cell volume of the daughter cell is
706 equal to half the volume of the parent cell, while the maturity buffer is emptied and the
707 maturity of the daughter cell is set to zero. The instantaneous growth rate (equation 21)
708 decreases during growth within a given cell cycle consistent with the fact that the growth rate
709 is proportional to the surface/volume ratio of cells. After a few cell cycles model variables
710 (structure, maturity, volume etc.) repeat themselves from one cycle to another: the model has
711 reached steady state. A full model run which brings the system into steady state lasts about
712 ten cell cycles. The final steady state condition is independent of the initial cell size and
713 depends only on nutrient concentrations and biological model parameters. The generation
714 time is graphically visible as the horizontal distance between two successive division events.
715 At steady state, the growth rate μ (in day^{-1}) can be approximated from the generation time G_T
716 (in days) (Powell, 1956):

$$717 \quad \mu = \frac{\log 2}{G_T} \quad (22)$$

718 The growth rate calculated from the generation time (equation 22) is numerically equivalent
719 to the average value of the instantaneous growth rate calculated with equation 21 (red dashed
720 line in figure 10c). In the following, I will discuss average cell volumes and growth rates at
721 steady state (dashed red lines in figures 10b and 10c).

722 Next, the model is used to investigate how cell-size and growth rate vary in conditions of
723 nutrient limitation. The model is run changing NO_3 and PO_4 concentrations while keeping all
724 the other model parameters unchanged. As explained above, the SUs were parameterized
725 such that NO_3 contributes primarily to the structure (and to a lesser extent to maturity) and
726 PO_4 contributes primarily to maturity (and to a lesser extent to the structure). The model was
727 run ten thousand times with combinations of NO_3 and PO_4 concentrations included between
728 10^{-2} to $1 \text{ mmol litre}^{-1}$ (NO_3) and 10^{-4} and $10^{-2} \text{ mmol litre}^{-1}$ (PO_4) (Figure 11). Figure 11a
729 shows how cell volume (blue contour lines) and growth rate (red dashed lines) depend on
730 NO_3 and PO_4 concentrations: while NO_3 and PO_4 limitation both result in a decrease of the

731 growth rate, they have contrasting effects on cell size, with NO₃ limitation resulting in a
 732 decrease size and PO₄ limitation in an increase of cell size. These trends are further displayed
 733 in figures 11b to 11e: figures 11b and 11c are plots of how growth rate and cell-size vary
 734 when PO₄ is kept at non-limiting levels (10⁻² mmol litre⁻¹) and NO₃ varies. Figures 11d and
 735 11e are plots of how growth rate and cell-size vary when NO₃ is kept at non-limiting levels (1
 736 mmol litre⁻¹) and PO₄ varies. Figures 11c and 11e are of the same sort of those presented in
 737 section 5 where changes in growth rate and cell volume induced by NO₃ and PO₄ limitation
 738 are represented on log scales. The experimental data from Riegman et al. (2000) (orange
 739 points: NO₃ limitation, brown points: PO₄ limitation) are included in figures 11c and 11e.

740 These simulations show that the model can reproduce trends in growth rate and cell size
 741 observed in laboratory experiments when NO₃ and PO₄ become limiting (section 5). In the
 742 following I discuss the features of the model that produce these trends. The growth rate is
 743 directly related to the generation time (equation 22). The generation time depends on the rate
 744 at which the maturity buffer is filled. Since both NO₃ and PO₄ contribute to the maturation
 745 flux, limitation in NO₃ and PO₄ both result in an increase in the generation time and a
 746 decrease in the growth rate. The link between growth rate and maturation flux is obvious if
 747 the maturation power is plotted as a function of NO₃ and PO₄ concentrations: the isolines of
 748 growth rate (figure 11a) follow those of the maturation power (figure 11b). Controls on cell
 749 size are slightly more complicated. Cell size is affected both by the rate of biomass increase
 750 and by the generation time. Specifically, cell size is proportional both to the rate of biomass
 751 increase and to the generation time (and thus inversely proportional to the growth rate). The
 752 key model quantity determining how the average cell size changes following a change in
 753 nutrient concentrations is the ratio of the energy fluxes dedicated to growth and maturation:
 754

$$755 \frac{\dot{P}_G}{\dot{P}_R} \quad (23)$$

756 Figure 11b shows the value of this ratio as a function of NO₃ and PO₄ concentrations. On a
 757 diagonal line along which NO₃ and PO₄ decrease by proportionally the same amount, the
 758 growth/maturity ratio is constant and equal to 1 and cell volume does not change (figure 11a).
 759 If NO₃ decreases more than PO₄, then growth is more affected than maturity, leading to a
 760 decrease in cell size, and vice versa.

761 We conclude that changes in simple model quantities, which have a sound basis in biological
762 metabolic theory, can explain the co-variance of metabolic rates and cell-size observed in
763 laboratory experiments where nitrate and phosphate are limiting. Although the model was run
764 with the uptake parameters of NO_3 and PO_4 , the same trend of growth rate and cell size
765 decrease with decreasing NO_3 concentrations is obtained if NO_3 is replaced by CO_2 , or the
766 Monod term for NO_3 is replaced by a Monod term for irradiance, suggesting that the simple
767 set of rules discussed here can potentially explain the majority of the trends in metabolic rates
768 and cell-size described in section 4. More work is needed to expand this simple physiological
769 model to include other important features of full DEB models such as the distinction between
770 reservoirs and structure, and to consider the interacting effect of multiple environmental
771 changes. There is hope, however, that this effort will be rewarded by a better understanding
772 of how environment affects the metabolic performance of coccolithophores in the modern
773 ocean - a fundamental step in predicting how this important group of phytoplankton will be
774 affected by climate change.

775

776 **7 Conclusions**

777 The examination of published results of coccolithophore culture experiments allows the
778 following conclusions. The scaling of coccolithophore metabolism to cell size in optimal
779 growth conditions is comparable to that observed in other phytoplankton groups by Marañón
780 (2008). Larger taxa experience greater photosynthesis and calcification rates, while the
781 growth rate is weakly dependent on cell-size. In addition cell size in *E. huxleyi* depends on
782 environmental conditions. When only one of pCO_2 , irradiance, temperature, NO_3 , PO_4 or Fe
783 is varied, cell-size and metabolic rates co-vary, defining clear trends in the 2D metabolism-
784 cell size space. An exception is calcification under variable pCO_2 that does not show clear
785 trends. The magnitude of coccosphere size changes observed by varying environmental
786 culture conditions in the laboratory is comparable to the variability of *E. huxleyi* coccosphere
787 size in the ocean. This suggests the existence of at least two controls on *E. huxleyi* cell size in
788 the ocean: 1) the change in the relative abundance of *E. huxleyi* morphotypes with different
789 characteristic cell sizes (*ecological control*) and 2) the change in coccosphere size induced by
790 fluctuating environmental conditions (*physiological control*). Simple rules that regulate the
791 partitioning of energy amongst growth and maturity explain the co-variance of cell-size and
792 metabolic rates observed in laboratory experiments. There is hope that the Dynamic Energy

793 Budget Theory - which formalizes this fundamental energy partitioning - can be used to
794 interpret coccosphere and coccolith cell-size in the past and modern ocean in terms of
795 environmental change, providing a key for predicting the fate of coccolithophores in the
796 future. In an evolutionary perspective, we can expect that adaptation to changing
797 environmental conditions will modulate the observed metabolism-cell size trends, adding
798 further complexity in the study of past and future response of coccolithophores to climate
799 change.

800

801

802

803

804

805

806

807

808

809

810

811

812

813

814

815

816

817

818 **Appendix**

819 **A1. The coccolithophore database**

820 The full coccolithophore database is presented in Table A1.

821 *Normalized cell carbon quota*

822 Due to cell division during the dark phase, POC at the end of the light phase (P_{END}) is double
823 the POC at the beginning of the light phase (P_0) :

824
$$POC_{END} = 2 \cdot POC_0 \quad (A1)$$

825 Thus, if POC increases linearly during the day, its evolution in time during the light phase
826 can be expressed as follows:

827
$$POC(t) = POC_0 + \frac{t}{L} \cdot POC_0 \quad (A2)$$

828 where t is time in hours and L is the length of the light period in hours. To obtain an
829 expression that calculates the carbon quota at any given time in the light phase, let S_T and
830 $POC(S_T)$ be the sampling time and the corresponding POC value measured in an experiment.
831 By substituting these values for $POC(t)$ and t in equation A2 and rearranging we can calculate
832 POC_0 :

833
$$POC_0 = \frac{L \cdot POC(S_T)}{L + S_T} \quad (A3)$$

834 We can then substitute this expression for POC_0 in equation A1 to obtain an expression
835 calculating the POC at any time during the light period:

836
$$POC(t) = \frac{L \cdot POC(S_T)}{L + S_T} \cdot \left(1 + \frac{t}{L}\right) \quad (A4)$$

837

838 *Estimating cell and coccosphere size from carbon quota*

839 The volume of the coccosphere can be thought of as the volume of the cell (V_{Cell}) plus that of
840 the coccolith shield (V_{Shield}) (see figure 1):

841 $V_{Sphere} = V_{Cell} + V_{Shield}$ (A5)

842 Both the cell and the shield contain water. Therefore, the volume of the cell can be expressed
843 as:

844 $V_{Cell} = V_{POM} + V_{H_2O_{Cell}}$ (A6)

845 where V_{POM} is the volume occupied by organic matter and $V_{H_2O_{Cell}}$ is the volume occupied by
846 water in the cell. Similarly, the volume of the shield can be expressed as:

847

848 $V_{Shield} = V_{CaCO_3} + V_{H_2O_{Shield}}$ (A7)

849 where V_{CaCO_3} is the volume of the $CaCO_3$ in all the coccoliths of the shield and $V_{H_2O_{Shield}}$ is
850 the volume of water contained in the shield. Defining f_{CY} and f_{SH} as the volume fractions of
851 water in the cell and shield, respectively, the volume of the coccosphere can be expressed as:

852

853 $V_{Sphere} = V_{POM} + \frac{f_{CY}}{1 - f_{CY}} \cdot V_{POM} + V_{CaCO_3} + \frac{f_{SH}}{1 - f_{SH}} \cdot V_{CaCO_3}$ (A8)

854 Expressing volumes in terms of mass divided by density, the above equation becomes:

855

856 $V_{Sphere} = \frac{M_{POM}}{d_{POM}} \cdot \left(1 + \frac{f_{CY}}{1 - f_{CY}}\right) + \frac{M_{CaCO_3}}{d_{CaCO_3}} \cdot \left(1 + \frac{f_{SH}}{1 - f_{SH}}\right)$ (A9)

857

858 where M_{POM} and M_{CaCO_3} are the mass of organic matter and $CaCO_3$ in the coccosphere,
859 respectively, and d_{POM} ($1.3 - 1.7 \text{ g cm}^{-3}$; (Walsby and Reynolds, 1980)) and d_{CaCO_3} (2.7 g cm^{-3})
860 are the density of organic matter and $CaCO_3$, respectively. M_{POM} is related to the organic
861 carbon per cell (POC) (Muller et al., 1986):

862

863 $M_{POM} = 1.8 \times POC$ (A10)

864 while the total mass of the coccoliths is related to the inorganic carbon content (PIC) per cell
865 by:

866
$$M_{CaCO_3} = \frac{MW_{CaCO_3}}{MW_C} \cdot PIC \quad (A11)$$

867 where MW_C is the molecular weight of carbon (12) and MW_{CaCO_3} is the molecular weight of
 868 $CaCO_3$ (100).

869 Substituting equations A10 and A11 in equation A9, the volume of the coccosphere can be
 870 expressed as:

871

872
$$V_{Sphere} = \frac{1.8 \times POC}{d_{POM}} \cdot \left(1 + \frac{f_{CY}}{1 - f_{CY}}\right) + \frac{100}{12} \cdot \frac{PIC}{d_{CaCO_3}} \cdot \left(1 + \frac{f_{Sh}}{1 - f_{Sh}}\right) \quad (A12)$$

873

874 As explained in section 2.4, the values chosen for f_{CY} (0.79) and f_{SH} (0.66) results in a
 875 difference between the diameter of the coccosphere and that of the cell of about 1.5 μm for
 876 most of *E. huxleyi* the cells. Values significantly smaller than 1.5 are observed when cells are
 877 cultured in Ca^{2+} -poor fluids (Riegman et al., 2000; Trimborn et al., 2007), low saturation
 878 states or undersaturation with respect to $CaCO_3$ (Bach et al., 2011; Borchard et al., 2011) or at
 879 very low light irradiances of 15 and 30 $\mu mol photons m^{-2} s^{-1}$ in (Zondervan et al., 2002). In
 880 one case (Feng et al., 2008) small values of the coccosphere-cell diameter difference occur at
 881 high irradiances (400 $\mu mol photons m^{-2} s^{-1}$) and are interpreted by these authors as reflecting
 882 inhibition of calcification at high irradiance. In three of the experiments carried out by (De
 883 Bodt et al., 2010), the coccosphere-cell diameter difference is roughly double ($\sim 3 \mu m$),
 884 suggesting the presence of two layers of coccoliths making up the shield that surrounds the
 885 cell.

886 The reconstruction of cell geometry obtained by applying equation 7 is compared to that
 887 obtained applying the equation of Montagnes et al. (1994) which relates cell carbon content
 888 (C, in $pg cell^{-1}$) to cell volume (V, in μm^3):

889
$$C = 0.109 \times V^{0.991} \quad (A13)$$

890

891 The diameter of *E. huxleyi* cells calculated with this formula is shown in figure 2a. The
892 resulting cell diameter is up to 1.5 μm larger than that obtained with equation 7. I decided to
893 use equation 7, rather than use the equation of Montagnes et al. (1994), because the equation
894 of Montagnes et al. (1994) implies a much lower density of carbon per cell ($0.1 \text{ pgC } \mu\text{m}^{-3}$)
895 and would result in *E. huxleyi* spheres larger (up to 12 μm diameter) than those observed in
896 culture and in the field. Similar to *E. huxleyi*, if the relation between cell volume and carbon
897 quota per cell of Montagnes et al. (1994) (equation A13) is applied to the *Coccolithus*
898 *braarudii* POC data, then the resulting coccosphere diameters for most of the coccospheres in
899 the database (20-25 μm) are higher than those reported in Henderiks (Henderiks, 2008) (18 –
900 22 μm) (Fig. 2c).

901 Figure 2 shows that the measured coccosphere diameter is always smaller than the
902 coccosphere diameter calculated with the geometric model (equation 7). The large majority
903 of coccosphere size measurements in the database were carried out with Coulter counters
904 (Table A2). It is known that cell-size measurements obtained with the coulter counter
905 underestimates the real coccosphere size as measured by scanning electron microscope
906 (SEM), possibly because the coulter counter does not see the coccolith shield (Oviedo et al.,
907 2014). Iglesias-Rodriguez et al. (2008) also report coccosphere size measurements obtained
908 with coulter counters that are significantly smaller those obtained with flow cytometry. In
909 fact, their coulter counter measurements are very similar to the flow cytometer measurements
910 after acidification of the sample, consistent with the idea that the coulter counter does not see
911 the coccolith shield (Oviedo et al., 2014). Similarly, by comparing light microscope
912 measurements with Coulter counter measurements van Rijssel and Gieskes (2002) report that
913 coulter counter does not see the coccosphere. These considerations seem to be confirmed by
914 the experiments of Langer et al. (2006) with *Calcidiscus leptoporus* for which the
915 coccosphere volume determined with equation 7 coincides with the SEM-derived volume
916 (without prior fixing of the cells).

917

918

919

920

921

922

923 Table A2 – Summary of methods used to determine the size of coccospheres in experiments
 924 included in the coccolithophore database

	Measurement type	Fixation reported	Notes
Müller et al. (2012)	CC ^a	no	Reports difference between non-acidified and acidified samples
Lefebvre et al. (2011)	FC ^b	no	
Borchard et al. (2011)	CC	no	
Bach et al. (2011)	CC	no	
Krug et al. (2011)	?	no	
Kaffes et al. (2010)	CC	no	
Fiorini et al. (2011)	CC	no	
De Bodt et al. (2010)	CC	yes	
Iglesias-Rodriguez et al. (2008)	CC and FC	yes, both	Coulter size << Cytometer size. Coulter = Cytometer after acidification
Langer et al. (2006)	SEM ^c	no	SEM-measured size coincides with size calculated with equation 7
Sciandra et al. (2003)	HOPC ^d and CC	no	HOPC results similar to CC results
Riegman et al. (2000)	CC	no	
van Rijssel and Gieskes (2002)	CC and LM ^e	no	LM measurement shows that coccosphere is not included in CC measurement
Arnold et al. (2013)	CC	no	

925 ^aCoulter counter, ^bFlow cytometer, ^cSEM, ^dHiac optical particle counter, ^eLight microscope.

926

927

928

929

930

931

932

933

934

935

936

937 **A2. Comparing the coccolithophore database with the Marañón (2008)**
938 **phytoplankton database**

939 Marañón (2008) reports metabolic rate measurements carried out in the field (via cell counts
940 and ^{14}C -radiolabelling during incubation experiments lasting a maximum of approximately 1
941 day) that are as far as possible representative of *in situ* rates. Further, he chose to plot data for
942 organisms growing in conditions of irradiance and nutrient availability that were more
943 favorable for growth, and ran incubations at *in situ* temperature. However, nutrient limitation
944 and sub-optimal irradiance conditions cannot be excluded for some of the measurements
945 included in his review (Marañón, personal communication). In his compilation, the
946 photosynthetic rates reported in units of $\text{pgC cell}^{-1} \text{h}^{-1}$ are converted in $\text{pgC cell}^{-1} \text{day}^{-1}$ by
947 multiplying by the length of the photoperiod that may be different for different locations.
948 When the length of the photoperiod was not available, Marañón (2008) used a photoperiod of
949 12h (Marañón, personal communication). In comparing the data of my dataset with the data
950 of Marañón (2008), I divided the instantaneous growth rate (μ_i) and cell-specific metabolic
951 rates (RPh_i and RCa_i) obtained with equations 5 and 6 by 2, obtaining rates that refer to a
952 photoperiod of 12h. Furthermore, I concentrate on the experiments from the coccolithophore
953 database that were carried out in culture conditions that presumably do not depart too much
954 from those of Marañón (2008). I thus selected 172 “optimum experiments” (Table 2) carried
955 out in conditions of high irradiance (\geq than $80 \mu\text{mol photons m}^2 \text{s}^{-1}$), nutrient replete
956 conditions (dissolved PO_4 and $\text{NO}_3 \geq 4$ and $64 \mu\text{M}$, respectively) and dissolved Ca between 9
957 and 11.3 mM . I further subdivided these optimum experiments in a “low pCO_2 ” sub-group,
958 with pCO_2 included between 150 and $550 \mu\text{atm}$ and total alkalinity between 2.1 and 2.45 mol
959 kg^{-1} , and a “high pCO_2 ” sub-group, with pCO_2 included between 551 and $1311 \mu\text{atm}$ and
960 total alkalinity between 1.9 and 2.6 mol kg^{-1} . The low pCO_2 sub-group is representative of
961 the ranges of the monthly means values of pCO_2 and total alkalinity in the surface ocean (Lee
962 et al., 2006; Takahashi, 2009). No distinction between low- pCO_2 and high- pCO_2 sub-groups
963 is made in section 3 where both groups are collectively referred to as the “optimum” group.
964 Instead, the low- pCO_2 and high pCO_2 subgroups are discussed separately and have distinct
965 symbols in the plots of section 4 and 5.

966

967

968 **A3. Comparison of changes in cell size with changes in metabolic rates**

969 *Method*

970 In section 4 the changes in cell-size and metabolic rates induced by a shift of a given
971 environmental parameter are discussed. For example, with regards to variations in pCO₂, I
972 singled out groups of culture experiments where pCO₂ was the only environmental parameter
973 that varied while all other culture and pre-culture conditions were reported to be constant. For
974 every such group of experiments I recorded the difference in cell volume and metabolic rates
975 between cells grown at a given pCO₂ and those of the experiment carried out at the lowest
976 pCO₂ level. For example, Langer et al. (2009) carried out four experiments with *E. huxleyi*
977 clone RCC 1238 at pCO₂ levels of 218, 412, 697 and 943 µatm. Except for the DIC
978 parameters that co-vary with pCO₂, all other pre-culture and experimental conditions were
979 the same. For this group of four experiments I calculated the difference in cell volume and
980 metabolic rates between the experiments at 412, 697 and 943 µatm and the experiment at 218
981 µatm, obtaining the displacement in the 2D volume-metabolism space for the three
982 experiments carried out at 412, 697 and 943 µatm.

983 *Irradiance and temperature changes*

984 Ideally, when comparing experiments at different irradiance and temperature levels, all other
985 experimental parameters should be constant. In the Zondervan et al. (2002) experiments I
986 selected couples of experiments with different irradiance and similar DIC system parameters.
987 Similarly, I compared experiments at different temperature but similar pCO₂ conditions in the
988 set of experiments by Sett et al. (2014). The difference in pCO₂ between different irradiance
989 or temperature conditions was never greater than 150 µatm. Given the effect of pCO₂ on cell-
990 size and metabolic rates (Fig. 5), some of the variability shown in the plots that show how
991 metabolic rates co-vary with cell-size when irradiance or temperature increases (Fig. 6) will
992 be due to variations in pCO₂.

993 *Nutrient limitation*

994 In Müller et al. (2012) the evolution in the 2D volume-metabolism space is obtained by
995 comparing nitrate-replete, batch and nitrate-limited chemostat experiments with comparable
996 DIC systems. In this way the only aquatic chemistry difference is in the dissolved nitrate
997 concentration. In the N-limited chemostat experiments of Riegman et al. (2000), the

998 displacement in the 2D size-metabolism space is obtained by the difference between the
999 highest growth rate (0.61 day^{-1}) and the nitrate-limited experiments that have lower growth
1000 rates (0.15 to 0.45 day^{-1}). In the semi-continuous cultures of Kaffes et al. (2010) the data
1001 obtained in NO_3 -replete conditions ($\sim 280 \mu\text{M}$) was compared with that obtained at “ambient”
1002 (N. Atlantic) NO_3 concentrations ($\sim 10 \mu\text{M}$). Similar to the nitrate-limited experiments of
1003 Riegman et al. (2000), in the P-limited experiment of Borchard et al. (2011) and Riegman et
1004 al. (2000), the displacement in the size-metabolism space is obtained by the difference of size
1005 and metabolism at the different dilution rates (which have different dissolved P
1006 concentrations).

1007 The shift in cell-size, growth and photosynthesis rate produced by iron limitation is deduced
1008 from the experiments of Schultz et al. (2007). These are batch experiments, so the growth
1009 rates estimated from cell counts are not reliable (Langer et al., 2013). Nevertheless, the iron-
1010 limited experiment was included because the batch experiments inform on the direction of
1011 change (positive or negative) of cell-size and metabolic rates. The net fixation rates in pmol
1012 $\text{cell}^{-1} \text{ hr}^{-1}$ measured by membrane-inlet mass spectrometry by Schultz et al. (2007) (their
1013 figure 3) were converted in $\text{pgC cell}^{-1} \text{ day}^{-1}$ considering 12 hours of light. The organic carbon
1014 quota per cell was then calculated from the carbon uptake rate and the growth rate (their table
1015 1) using equation 5. The shift in metabolic rates and cell-size for iron limitation was obtained
1016 from the difference between the iron-replete and iron-limited experiments.

1017 *Increase in $p\text{CO}_2$ in nitrate-limited conditions*

1018 The evolution in the metabolism-volume space following an increase in $p\text{CO}_2$ in nutrient-
1019 limited conditions is hard to assess. Ideally, when $p\text{CO}_2$ is changed in the chemostat, the
1020 dilution rate should be adjusted so that the nutrient concentration remains unaltered. In this
1021 way, two nutrient-limited chemostat experiments with different $p\text{CO}_2$ levels could be
1022 compared. To the best of my knowledge this has not been done. However, the results of
1023 Müller et al. (2012) suggest that the growth rate changes little with $p\text{CO}_2$ in conditions of
1024 nitrate limitation. In these experiments, the cell-size and cell-specific photosynthesis rate of
1025 nitrate-limited cells increases with $p\text{CO}_2$. Nitrate is below the detection limit in all of these
1026 chemostat experiments. However, the extent to which the N/C ratio is lower in nitrate-
1027 depleted cells compared to nitrate-replete cells does not vary with $p\text{CO}_2$. Since decreased
1028 biomass N/C ratios are an indication of the extent of nitrate-limitation, we can conclude that
1029 the level of limitation is similar in the nitrate-limited experiments. With this in mind, the

1030 behavior of the cells in the Müller et al. (2012) experiment is comparable to that of the cell
1031 which experience a pCO₂ increase in optimum conditions: little or no change in the growth
1032 rate, an increase in rate of photosynthesis and a decreased in calcification.

1033

1034 **A4. Limitations of the simple DEB approach**

1035 Proper DEB models of dividing unicellular organisms are more complex than the simple
1036 version introduced in section 6. Specifically, 1) full DEB models include reserves, as well as
1037 structure and maturity, so that uptake and assimilation are decoupled and biomass
1038 stoichiometry varies with changes in nutrient availability (stoichiometry is fixed in the model
1039 used in this manuscript), 2) full DEB models consider the energy flow devoted to somatic
1040 maintenance and maturity maintenance, 3) part of the energy rejected by the growth SU is re-
1041 absorbed into the reserves in full DEB models. Notwithstanding these limitations, the simple
1042 model presented in this manuscript has the minimum characteristics of DEB models that are
1043 necessary to reproduce typical co-variations of metabolic rates and cell size.

1044

1045 **Acknowledgements**

1046 Rosalind Rickaby, Marius Müller and Jorijntje Henderiks provided access to part of the data
1047 included in the coccolithophore database. Emilio Marañón provided information on his
1048 database on phytoplankton physiology that permits the comparison with the coccolithophore
1049 database presented in this manuscript. Jorijntje Henderiks and Patrizia Ziveri provided useful
1050 comments on this manuscript.

1051

1052

1053

1054

1055

1056

1057

1058

1059

1060

1061 REFERENCES

1062

- 1063 Arnold, H. E., Kerrison, P., and Steinke, M.: Interacting effects of ocean acidification and warming on
 1064 growth and DMS-production in the haptophyte coccolithophore *Emiliana huxleyi*, *Global Change*
 1065 *Biology*, 19, 1007-1016, 2013.
- 1066 Atkinson, D., Ciotti, B. J., and Montagnes, D. J. S.: Protists decrease in size linearly with temperature:
 1067 ca. 2.5% C⁻¹, *Proceedings of the Royal Society B: Biological Sciences*, 270, 2605-2611, 2003.
- 1068 Bach, L. T., Bauke, C., Meier, K. J. S., Riebesell, U., and Schulz, K. G.: Influence of changing carbonate
 1069 chemistry on morphology and weight of coccoliths formed by *Emiliana huxleyi*,
 1070 *Biogeosciences*, 9, 3449-3463, 2012.
- 1071 Bach, L. T., Riebesell, U., and Georg Schulz, K.: Distinguishing between the effects of ocean
 1072 acidification and ocean carbonation in the coccolithophore *Emiliana huxleyi*, *Limnol. Oceanogr.*,
 1073 56, 2040-2050, 2011.
- 1074 Bach, L. T., Riebesell, U., Gutowska, M. A., Federwisch, L., and Schulz, K. G.: A unifying concept of
 1075 coccolithophore sensitivity to changing carbonate chemistry embedded in an ecological
 1076 framework, *Prog Oceanogr*, 135, 125-138, 2015.
- 1077 Banavar, J. R., Damuth, J., Maritan, A., and Rinaldo, A.: Supply-demand balance and metabolic
 1078 scaling, *Proceedings of the National Academy of Sciences*, 99, 10506-10509, 2002.
- 1079 Beaufort, L., Couapel, M., Buchet, N., Claustre, H., and Goyet, C.: Calcite production by
 1080 coccolithophores in the south east Pacific Ocean, *Biogeosciences*, 5, 1101-1117, 2008.
- 1081 Beaufort, L., Probert, I., de Garidel-Thoron, T., Bendif, E. M., Ruiz-Pino, D., Metzl, N., Goyet, C.,
 1082 Buchet, N., Coupel, P., Grelaud, M., Rost, B., Rickaby, R. E. M., and de Vargas, C.: Sensitivity of
 1083 coccolithophores to carbonate chemistry and ocean acidification, *Nature*, 476, 80-83, 2011.
- 1084 Behrenfeld, M. J., O'Malley, R. T., Siegel, D. A., McClain, C. R., Sarmiento, J. L., Feldman, G. C.,
 1085 Milligan, A. J., Falkowski, P. G., Letelier, R. M., and Boss, E. S.: Climate-driven trends in
 1086 contemporary ocean productivity, *Nature*, 444, 752-755, 2006.
- 1087 Berger, C., Meier, K. J. S., Kinkel, H., and Baumann, K. H.: Changes in calcification of coccoliths under
 1088 stable atmospheric CO₂, *Biogeosciences*, 11, 929-944, 2014.
- 1089 Bollmann, J. and Herrle, J. O.: Morphological variation of *Emiliana huxleyi* and sea surface salinity,
 1090 *Earth and Planetary Science Letters*, 255, 273-288, 2007.
- 1091 Bolton, C. T. and Stoll, H. M.: Late Miocene threshold response of marine algae to carbon dioxide
 1092 limitation, *Nature*, 500, 558-562, 2013.
- 1093 Bopp, L.: Response of diatoms distribution to global warming and potential implications: A global
 1094 model study, *Geophysical Research Letters*, 32, 2005.
- 1095 Bopp, L., Monfray, P., Aumont, O., Dufresne, J.-L., Le Treut, H., Madec, G., Terray, L., and Orr, J. C.:
 1096 Potential impact of climate change on marine export production, *Glob. Biogeochem. Cycle*, 15,
 1097 81-99, 2001.
- 1098 Borchard, C., Borges, A. V., Händel, N., and Engel, A.: Biogeochemical response of *Emiliana huxleyi*
 1099 (PML B92/11) to elevated CO₂ and temperature under phosphorous limitation: A chemostat
 1100 study, *J. Exp. Mar. Biol. Ecol.*, 2011.
- 1101 Broecker, W. and Clark, E.: Ratio of coccolith CaCO₃ to foraminifera CaCO₃ in late Holocene deep
 1102 sea sediments, *Paleoceanography*, 24, 2009.
- 1103 Brownlee, C., Davis, M., Nimer, N., Dong, L. F., and Merret, M. J.: Calcification, photosynthesis and
 1104 intracellular regulation of *Emiliana huxleyi*, *Bulletin de l'Institut Océanographique de Monaco*,
 1105 14, 19-35, 1995.
- 1106 Cermeño, P., Marañón, E., Harbour, D., and Harris, R. P.: Invariant scaling of phytoplankton
 1107 abundance and cell size in contrasting marine environments, *Ecol Lett*, 9, 1210-1215, 2006.
- 1108 Cook, S. S., Whittock, L., Wright, S. W., and Hallegraeff, G. M.: Photosynthetic pigment and genetic
 1109 differences between two southern ocean morphotypes of *emiliana huxleyi* (haptophyta), *Journal*
 1110 *of Phycology*, 47, 615-626, 2011.

- 1111 Cubillos, J. C., Wright, S. W., Nash, G., de Salas, M. F., Griffiths, B., Tilbrook, B., Poisson, A., and
1112 Hallegraeff, G. M.: Calcification morphotypes of the coccolithophorid *Emiliana huxleyi* in the
1113 Southern Ocean: changes in 2001 to 2006 compared to historical data, *Marine Ecology Progress
1114 Series*, 348, 47-54, 2007.
- 1115 De Bodt, C., Van Oostende, N., Harlay, J., Sabbe, K., and Chou, L.: Individual and interacting effects of
1116 pCO₂ and temperature on *Emiliana huxleyi* calcification: study of the calcite production, the
1117 coccolith morphology and the coccosphere size, *Biogeosciences*, 7, 1401-1412, 2010.
- 1118 Feng, Y., Warner, M. E., Zhang, Y., Sun, J., Fu, F.-X., Rose, J. M., and Hutchins, D. A.: Interactive
1119 effects of increased pCO₂, temperature and irradiance on the marine
1120 coccolithophore *Emiliana huxleyi* (Prymnesiophyceae), *European Journal of
1121 Phycology*, 43, 87 - 98, 2008.
- 1122 Fiorini, S., Middelburg, J. J., and Gattuso, J.-P.: Testing the Effects of Elevated Pco₂ on
1123 Coccolithophores (Prymnesiophyceae): Comparison between Haploid and Diploid Life Stages1,
1124 *Journal of Phycology*, no-no, 2011.
- 1125 Gehlen, M., Gangsto, R., Schneider, B., Bopp, L., Aumont, O. and Ethe, C. : The fate of pelagic CaCO₃
1126 production in a high CO₂ ocean: a model study, *Biogeosciences*, 4, 505-519, 2007.
- 1127 Geider, R. and La Roche, J.: Redfield revisited: variability of C:N:P in marine microalgae and its
1128 biochemical basis, *European Journal of Phycology*, 37, 1-17, 2002.
- 1129 Grelaud, M., Schimmelmann, A., and Beaufort, L.: Coccolithophore response to climate and surface
1130 hydrography in Santa Barbara Basin, California, AD 1917-2004, *Biogeosciences*, 6, 2025-2039,
1131 2009.
- 1132 Hagino, K., Okada, H., and Matsuoka, H.: Coccolithophore assemblages and morphotypes of
1133 *Emiliana huxleyi* in the boundary zone between the cold Oyashio and warm Kuroshio currents off
1134 the coast of Japan, *Marine Micropaleontology*, 55, 19-47, 2005.
- 1135 Henderiks, J.: Coccolithophore size rules - Reconstructing ancient cell geometry and cellular calcite
1136 quota from fossil coccoliths, *Marine Micropaleontology*, 67, 143-154, 2008.
- 1137 Henderiks, J., Winter, A., Elbrächter, M., Feistel, R., der Plas, A., Nausch, G., and Barlow, R.:
1138 Environmental controls on *Emiliana huxleyi* morphotypes in the Benguela coastal upwelling
1139 system (SE Atlantic), *Marine Ecology Progress Series*, 448, 51-66, 2012.
- 1140 Honjo, S., Manganini, S. J., Krishfield, R. A., and Francois, R.: Particulate organic carbon fluxes to the
1141 ocean interior and factors controlling the biological pump: A synthesis of global sediment trap
1142 programs since 1983, *Prog Oceanogr*, 76, 217-285, 2008.
- 1143 Hoppe, C. J. M., Langer, G., and Rost, B.: *Emiliana huxleyi* shows identical responses to elevated
1144 pCO₂ in TA and DIC manipulations, *J. Exp. Mar. Biol. Ecol.*, 406, 54-62, 2011.
- 1145 Horigome, M. T., Ziveri, P., Grelaud, M., Baumann, K. H., Marino, G., and Mortyn, P. G.:
1146 Environmental controls on the *Emiliana huxleyi* calcite mass, *Biogeosciences*, 11, 2295-
1147 2308, 2014.
- 1148 Huete-Ortega, M., Cermeno, P., Calvo-Diaz, A., and Marañón, E.: Isometric size-scaling of metabolic
1149 rate and the size abundance distribution of phytoplankton, *Proceedings of the Royal Society B:
1150 Biological Sciences*, 279, 1815-1823, 2012.
- 1151 Iglesias-Rodríguez, D. M., Schofield, O. M., Batley, J., Medlin, L. K., and Hayes, P. K.: Intraspecific
1152 genetic diversity in the marine coccolithophore *emiliana huxleyi* (prymnesiophyceae): the use of
1153 microsatellite analysis in marine phytoplankton population studies1, *Journal of Phycology*, 42,
1154 526-536, 2006.
- 1155 Iglesias-Rodríguez, M. D.: Representing key phytoplankton functional groups in ocean carbon cycle
1156 models: Coccolithophorids, *Glob. Biogeochem. Cycle*, 16, 2002.
- 1157 Iglesias-Rodríguez, M. D., Halloran, P. R., Rickaby, R. E. M., Hall, I. R., Colmenero-Hidalgo, E., Gittins,
1158 J. R., Green, D. R. H., Tyrrell, T., Gibbs, S. J., von Dassow, P., Rehm, E., Armbrust, E. V., and
1159 Boessenkool, K. P.: Phytoplankton calcification in a high-CO₂ world, *Science*, 320, 336-340, 2008.

1160 Kaffes, A., Thoms, S., Trimborn, S., Rost, B., Langer, G., Richter, K.-U., Köhler, A., Norici, A., and
1161 Giordano, M.: Carbon and nitrogen fluxes in the marine coccolithophore *Emiliana huxleyi* grown
1162 under different nitrate concentrations, *J. Exp. Mar. Biol. Ecol.*, 393, 1-8, 2010.

1163 Kooijman, S. A. L. M.: *Dynamic Energy Budget Theory for Metabolic Organisation*, Cambridge
1164 University Press, Cambridge, 2010.

1165 Krug, S. A., Schulz, K. G., and Riebesell, U.: Effects of changes in carbonate chemistry speciation on
1166 *Coccolithus braarudii*: a discussion of coccolithophorid sensitivities, *Biogeosciences*, 8,
1167 771-777, 2011.

1168 Langer, G., Geisen, M., Baumann, K. H., Klas, J., Riebesell, U., Thoms, S., and Young, J. R.: Species-
1169 specific responses of calcifying algae to changing seawater carbonate chemistry, *Geochem.*
1170 *Geophys. Geosyst.*, 7, 2006.

1171 Langer, G., Nehrke, G., Probert, I., Ly, J., and Ziveri, P.: Strain-specific responses of *Emiliana huxleyi*
1172 to changing seawater carbonate chemistry, *Biogeosciences* 6, 2637-2646, 2009.

1173 Langer, G., Oetjen, K., and Brenneis, T.: Calcification of *Calcidiscus leptoporus* under nitrogen and
1174 phosphorus limitation, *J. Exp. Mar. Biol. Ecol.*, 413, 131-137, 2012.

1175 Langer, G., Oetjen, K., and Brenneis, T.: Coccolithophores do not increase particulate carbon
1176 production under nutrient limitation: A case study using *Emiliana huxleyi* (PML B92/11), *J. Exp.*
1177 *Mar. Biol. Ecol.*, 443, 155-161, 2013.

1178 LaRoche, J., Rost, B., and Engel, A.: Bioassays, batch culture and chemostat experimentation. In:
1179 Guide of best practices for ocean acidification research and data processing, Riebesell, U., Fabry,
1180 V. J., Hansson, L., and Gattuso, J.-P. (Eds.), Publications office of the European Union,
1181 Luxembourg, 2010.

1182 Laws, E. A. and Bannister, T. T.: Nutrient-Limited and Light-Limited Growth of *Thalassiosira-Fluviatilis*
1183 in Continuous Culture, with Implications for Phytoplankton Growth in the Ocean, *Limnol.*
1184 *Oceanogr.*, 25, 457-473, 1980.

1185 Lee, K., Tong, L. T., Millero, F. J., Sabine, C. L., Dickson, A. G., Goyet, C., Park, G.-H., Wanninkhof, R.,
1186 Feely, R. A., and Key, R. M.: Global relationships of total alkalinity with salinity and temperature in
1187 surface waters of the world's oceans, *Geophysical Research Letters*, 33, 2006.

1188 Lefebvre, S. C., Benner, I., Stillman, J. H., Parker, A. E., Drake, M. K., Rossignol, P. E., Okimura, K. M.,
1189 Komada, T., and Carpenter, E. J.: Nitrogen source and pCO₂ synergistically affect carbon
1190 allocation, growth and morphology of the coccolithophore *Emiliana huxleyi*: potential
1191 implications of ocean acidification for the carbon cycle, *Global Change Biology*, n/a-n/a, 2011.

1192 Linschooten, C., Vanbleijswijk, J. D. L., Vanenburg, P. R., Devrind, J. P. M., Kempers, E. S., Westbroek,
1193 P., and Devrinddejong, E. W.: Role of the Light-Dark Cycle and Medium Composition on the
1194 Production of Coccoliths by *Emiliana-Huxleyi* (Haptophyceae), *Journal of Phycology*, 27, 82-86,
1195 1991.

1196 Lohbeck, K. T., Riebesell, U., and Reusch, T. B. H.: Adaptive evolution of a key phytoplankton species
1197 to ocean acidification, *Nature Geoscience*, 2012.

1198 López-Sandoval, D. C., Rodríguez-Ramos, T., Cermeño, P., Sobrino, C., and Marañón, E.:
1199 Photosynthesis and respiration in marine phytoplankton: Relationship with cell size, taxonomic
1200 affiliation, and growth phase, *J. Exp. Mar. Biol. Ecol.*, 457, 151-159, 2014.

1201 Lopez-Urrutia, A., San Martin, E., Harris, R.P. and Irigoien, X.: Scaling the metabolic balance of the
1202 oceans, *Proceedings of the National Academy of Sciences*, 103, 8739-8744, 2006.

1203 Lorena, A., Marques, G. M., Kooijman, S. A. L. M., and Sousa, T.: Stylized facts in microalgal growth:
1204 interpretation in a dynamic energy budget context, *Philosophical Transactions of the Royal*
1205 *Society B: Biological Sciences*, 365, 3509-3521, 2010.

1206 Marañón, E.: Inter-specific scaling of phytoplankton production and cell size in the field, *Journal of*
1207 *Plankton Research*, 30, 157-163, 2008.

1208 Marañón, E., Cermeño, P., López-Sandoval, D. C., Rodríguez-Ramos, T., Sobrino, C., Huete-Ortega,
1209 M., Blanco, J. M., Rodríguez, J., and Fussmann, G.: Unimodal size scaling of phytoplankton growth
1210 and the size dependence of nutrient uptake and use, *Ecol Lett*, 16, 371-379, 2013.

1211 Marañón, E., Cermeño, P., Rodriguez, J., Zubkov, M. V., and Harris, R. P.: Scaling of phytoplankton
1212 photosynthesis and cell size in the ocean, *Limnol. Oceanogr.*, 52, 2190-2198, 2007.

1213 Medlin, L. K., Barker, G. L. A., Campbell, L., Green, J. C., Hayes, P. K., Marie, D., Wrieden, S., and
1214 Vault, D.: Genetic characterisation of *Emiliana huxleyi* (Haptophyta), *Journal of Marine Systems*,
1215 9, 13-31, 1996.

1216 Meier, K. J. S., Beaufort, L., Heussner, S., and Ziveri, P.: The role of ocean acidification in *Emiliana*
1217 *huxleyi* coccolith thinning in the Mediterranean Sea, *Biogeosciences*, 11, 2857-2869, 2014.

1218 Menden-Deuer, S. and Lessard, E. J.: Carbon to volume relationships for Dinoflagellates, Diatoms,
1219 and other protist plankton, *Limnol. Oceanogr.*, 45, 569-579, 2000.

1220 Mitrovic, S. M., Howden, C. G., and Bowling, L. C.: Unusual allometry between in situ growth of
1221 freshwater phytoplankton under static and fluctuating light environments: possible implications
1222 for dominance, *Journal of Plankton Research*, 25, 517-526, 2005.

1223 Montagnes, D. J. S., Berges, J. A., Harrison, P. J., and Taylor, F. J. R.: Estimating Carbon, Nitrogen,
1224 Protein, and Chlorophyll-a from Volume in Marine-Phytoplankton, *Limnol. Oceanogr.*, 39, 1044-
1225 1060, 1994.

1226 Muller, E. B., Ananthasubramaniam, B., Klanjšček, T., and Nisbet, R. M.: Entrainment of cell division
1227 in phytoplankton with dynamic energy budgets, *Journal of Sea Research*, 66, 447-455, 2011.

1228 Muller, E. B. and Nisbet, R. M.: Dynamic energy budget modeling reveals the potential of future
1229 growth and calcification for the coccolithophore *Emiliana huxleyi* in an acidified ocean, *Global*
1230 *Change Biology*, 20, 2031-2038, 2014.

1231 Muller, M. N., Antia, A. N., and LaRoche, J.: Influence of cell cycle phase on calcification in the
1232 coccolithophore *Emiliana huxleyi*, *Limnol. Oceanogr.*, 53, 506-512, 2008.

1233 Müller, M. N., Beaufort, L., Bernard, O., Pedrotti, M. L., Talec, A., and Sciandra, A.: Influence of
1234 CO₂ and nitrogen limitation on the coccolith volume of *Emiliana huxleyi*
1235 (Haptophyta), *Biogeosciences Discussions*, 9, 4979-5010, 2012.

1236 Muller, P. J., Suess, E., and Ungerer, C. A.: Amino-Acids and Amino-Sugars of Surface Particulate and
1237 Sediment Trap Material from Waters of the Scotia Sea, *Deep-Sea Res*, 33, 819-838, 1986.

1238 Niklas, K. J. and Enquist, B. J.: Invariant scaling relationships for interspecific plant biomass
1239 production rates and body size, *Proceedings of the National Academy of Sciences*, 98, 2922-2927,
1240 2001.

1241 Oviedo, A. M., Langer, G., and Ziveri, P.: Effect of phosphorus limitation on coccolith morphology and
1242 element ratios in Mediterranean strains of the coccolithophore *Emiliana huxleyi*, *J. Exp. Mar.*
1243 *Biol. Ecol.*, 459, 105-113, 2014.

1244 Paasche, E.: Marine plankton algae grown with light-dark cycles. I. *Coccolithus huxleyi*, *Physiologia*
1245 *Plantarum*, 20, 946-956, 1967.

1246 Paasche, E.: Reduced coccolith calcite production under light-limited growth: a comparative study of
1247 three clones of *Emiliana huxleyi* (Prymnesiophyceae), *Phycologia*, 38, 508-516, 1999.

1248 Paasche, E.: A review of the coccolithophorid *Emiliana huxleyi* (Prymnesiophyceae), with particular
1249 reference to growth, coccolith formation, and calcification-photosynthesis interactions,
1250 *Phycologia*, 40, 503-529, 2001.

1251 Paasche, E., Brubak, S., Skattebol, S., Young, J. R., and Green, J. C.: Growth and calcification in the
1252 coccolithophorid *Emiliana huxleyi* (Haptophyceae) at low salinities, *Phycologia*, 35, 394-403,
1253 1996.

1254 Poulton, A. J., Adey, T. R., Balch, W. M., and Holligan, P. M.: Relating coccolithophore calcification
1255 rates to phytoplankton community dynamics: Regional differences and implications for carbon
1256 export, *Deep Sea Research Part II: Topical Studies in Oceanography*, 54, 538-557, 2007.

1257 Poulton, A. J., Stinchcombe, M. C., Achterberg, E. P., Bakker, D. C. E., Dumousseaud, C., Lawson, H.
1258 E., Lee, G. A., Richier, S., Suggett, D. J., and Young, J. R.: Coccolithophores on the north-west
1259 European shelf: calcification rates and environmental controls, *Biogeosciences Discussions*, 11,
1260 2685-2733, 2014.

1261 Poulton, A. J., Young, J. R., Bates, N. R., and Balch, W. M.: Biometry of detached *Emiliana huxleyi*
1262 coccoliths along the Patagonian Shelf, *Marine Ecology Progress Series*, 443, 1-17, 2011.

1263 Powell, E. O.: Growth rate and generation time of bacteria, with special reference to continuous
1264 culture, *Journal of General Microbiology*, 15, 492-511, 1956.

1265 Raven, J. A.: The twelfth Tansley Lecture. Small is beautiful: the picophytoplankton, *Functional*
1266 *Ecology*, 12, 503-513, 1998.

1267 Raven, J. A. and Crawford, K.: Environmental controls on coccolithophore calcification, *Marine*
1268 *Ecology Progress Series*, 470, 137-166, 2012.

1269 Read, B. A., Kegel, J., Klute, M. J., Kuo, A., Lefebvre, S. C., Maumus, F., Mayer, C., Miller, J., Monier,
1270 A., Salamov, A., Young, J., Aguilar, M., Claverie, J.-M., Frickenhaus, S., Gonzalez, K., Herman, E. K.,
1271 Lin, Y.-C., Napier, J., Ogata, H., Sarno, A. F., Shmutz, J., Schroeder, D., de Vargas, C., Verret, F., von
1272 Dassow, P., Valentin, K., Van de Peer, Y., Wheeler, G., Dacks, J. B., Delwiche, C. F., Dyrman, S. T.,
1273 Gloeckner, G., John, U., Richards, T., Worden, A. Z., Zhang, X., Grigoriev, I. V., Allen, A. E., Bidle, K.,
1274 Borodovsky, M., Bowler, C., Brownlee, C., Cock, J. M., Elias, M., Gladyshev, V. N., Groth, M., Guda,
1275 C., Hadaegh, A., Iglesias-Rodríguez, M. D., Jenkins, J., Jones, B. M., Lawson, T., Leese, F., Lindquist,
1276 E., Lobanov, A., Lomsadze, A., Malik, S.-B., Marsh, M. E., Mackinder, L., Mock, T., Mueller-Roeber,
1277 B., Pagarete, A., Parker, M., Probert, I., Quesneville, H., Raines, C., Rensing, S. A., Riano-Pachon,
1278 D. M., Richier, S., Rokitta, S., Shiraiwa, Y., Soanes, D. M., van der Giezen, M., Wahlund, T. M.,
1279 Williams, B., Wilson, W., Wolfe, G., Wurch, L. L., and *Emiliana Huxleyi*, A.: Pan genome of the
1280 phytoplankton *Emiliana* underpins its global distribution, *Nature*, 499, 209-213, 2013.

1281 Reinfelder, J. R.: Carbon Concentrating Mechanisms in Eukaryotic Marine Phytoplankton, *Annual*
1282 *Review of Marine Science*, 3, 291-315, 2011.

1283 Riebesell, U., Zondervan, I., Rost, B., Tortell, P. D., Zeebe, R. E., and Morel, F. M. M.: Reduced
1284 calcification of marine plankton in response to increased atmospheric CO₂, *Nature*, 407, 364-367,
1285 2000.

1286 Riegman, R., Stolte, W., Noordeloos, A. A. M., and Slezak, D.: Nutrient uptake, and alkaline
1287 phosphate (EC 3 : 1 : 3 : 1) activity of *Emiliana huxleyi* (Prymnesiophyceae) during growth under
1288 N and P limitation in continuous cultures, *Journal of Phycology*, 36, 87-96, 2000.

1289 Rokitta, S. D. and Rost, B.: Effects of CO₂ and their modulation by light in the life-cycle stages of the
1290 coccolithophore *Emiliana huxleyi*, *Limnol. Oceanogr.*, 57, 607-618, 2012.

1291 Rost, B., Riebesell, U., Burkhardt, S., and Sultemeyer, D.: Carbon acquisition of bloom-forming
1292 marine phytoplankton, *Limnol. Oceanogr.*, 48, 55-67, 2003.

1293 Rost, B., Zondervan, I., and Riebesell, U.: Light-dependent carbon isotope fractionation in the
1294 coccolithophorid *Emiliana huxleyi*, *Limnol. Oceanogr.*, 47, 120-128, 2002.

1295 Rouco, M., Branson, O., Lebrato, M., and Iglesias-Rodríguez, M. D.: The effect of nitrate and
1296 phosphate availability on *Emiliana huxleyi* (NZEH) physiology under different CO₂ scenarios,
1297 *Frontiers in Microbiology*, 4, 2013.

1298 Satoh, M., Iwamoto, K., Suzuki, I., and Shiraiwa, Y.: Cold Stress Stimulates Intracellular Calcification
1299 by the Coccolithophore, *Emiliana huxleyi* (Haptophyceae) Under Phosphate-Deficient Conditions,
1300 *Mar. Biotechnol.*, 11, 327-333, 2008.

1301 Schiebel, R., Brupbacher, U., Schmidtko, S., Nausch, G., Waniek, J. J., and Thierstein, H.-R.: Spring
1302 coccolithophore production and dispersion in the temperate eastern North Atlantic Ocean,
1303 *Journal of Geophysical Research*, 116, 2011.

1304 Schlüter, L., Lohbeck, K. T., Gutowska, M. A., Gröger, J. P., Riebesell, U., and Reusch, T. B. H.:
1305 Adaptation of a globally important coccolithophore to ocean warming and acidification, *Nature*
1306 *Climate Change*, 2014.

1307 Schroeder, D. C., Biggi, G. F., Hall, M., Davy, J., Martínez, J. M., Richardson, A. J., Malin, G., and
1308 Wilson, W. H.: A genetic marker to separate *emiliana huxleyi* (prymnesiophyceae) morphotypes,
1309 *Journal of Phycology*, 41, 874-879, 2005.

1310 Schulz, K. G., Rost, B., Burkhardt, S., Riebesell, U., Thoms, S., and Wolf-Gladrow, D. A.: The effect of
1311 iron availability on the regulation of inorganic carbon acquisition in the coccolithophore *Emiliana*

1312 huxleyi and the significance of cellular compartmentation for stable carbon isotope fractionation,
1313 Geochim. Cosmochim. Acta, 71, 5301-5312, 2007.

1314 Sciandra, A., Harlay, J., Lefevre, D., Lemee, R., Rimmelin, P., Denis, M., and Gattuso, J. P.: Response
1315 of coccolithophorid *Emiliana huxleyi* to elevated partial pressure of CO₂ under nitrogen
1316 limitation, Marine Ecology-Progress Series, 261, 111-122, 2003.

1317 Sett, S., Bach, L. T., Schulz, K. G., Koch-Klavsen, S., Lebrato, M., and Riebesell, U.: Temperature
1318 Modulates Coccolithophorid Sensitivity of Growth, Photosynthesis and Calcification to Increasing
1319 Seawater pCO₂, PLoS ONE, 9, e88308, 2014.

1320 Shutler, J. D., Land, P. E., Brown, C. W., Findlay, H. S., Donlon, C. J., Medland, M., Snooke, R., and
1321 Blackford, J. C.: Coccolithophore surface distributions in the North Atlantic and their modulation
1322 of the air-sea flux of CO₂ from 10 years of satellite Earth observation data,
1323 Biogeosciences, 10, 2699-2709, 2013.

1324 Smith, H. E. K., Tyrrell, T., Charalampopoulou, A., Dumousseaud, C., Legge, O. J., Birchenough, S.,
1325 Pettit, L. R., Garley, R., Hartman, S. E., Hartman, M. C., Sagoo, N., Daniels, C. J., Achterberg, E. P.,
1326 and Hydes, D. J.: Predominance of heavily calcified coccolithophores at low CaCO₃ saturation
1327 during winter in the Bay of Biscay, Proceedings of the National Academy of Sciences, 109, 8845-
1328 8849, 2012.

1329 Stolte, W., McCollin, T., and Noordeloos, A. M.: Effect of nitrogen source on the size distribution
1330 within marine phytoplankton populations, J. Exp. Mar. Biol. Ecol., 184, 83-97, 1994.

1331 Takahashi, T.: Climatological mean and decadal change in surface ocean pCO₂, and net sea-air CO₂
1332 flux over the global oceans, Deep Sea Research Part II: Topical Studies in Oceanography, 56, 554-
1333 577, 2009.

1334 Thomas, M. K., Kremer, C. T., Klausmeier, C. A., and Litchman, E.: A global pattern of thermazl
1335 adaptation in marine phytoplankton, Science, 338, 1085-1088, 2012.

1336 Trimborn, S., Langer, G., and Rost, B.: Effect of varying calcium concentrations and light intensities
1337 on calcification and photosynthesis in *Emiliana huxleyi*, Limnol. Oceanogr., 52, 2285-2293, 2007.

1338 van Rijssel, M. and Gieskes, W. W. C.: Temperature, light, and the dimethylsulfoniopropionate
1339 (DMSP) content of *Emiliana huxleyi* (Prymnesiophyceae), Journal of Sea Research, 48, 2002.

1340 Vanbleijswijk, J. D. L., Kempers, R. S., Veldhuis, M. J., and Westbroek, P.: Cell and Growth-
1341 Characteristics of Type-a and Type-B of *Emiliana-Huxleyi* (Prymnesiophyceae) as Determined by
1342 Flow-Cytometry and Chemical-Analyses, Journal of Phycology, 30, 230-241, 1994.

1343 Walsby, A. F. and Reynolds, C. S.: Sinking and floating. In: The physiological ecology of
1344 phytoplankton, Morris, I. (Ed.), University of California Press, Berkeley, 1980.

1345 West, G. B., Brown, J. H., and Enquist, B. J.: A general model for the origin of allometric scaling laws
1346 in biology, Science, 276, 122-126, 1997.

1347 Wilson, J. D., Barker, S., and Ridgwell, A.: Assessment of the spatial variability in particulate organic
1348 matter and mineral sinking fluxes in the ocean interior: Implications for the ballast hypothesis,
1349 Glob. Biogeochem. Cycle, 26, 2012.

1350 Winter, A., Henderiks, J., Beaufort, L., Rickaby, R. E. M., and Brown, C. W.: Poleward expansion of the
1351 coccolithophore *Emiliana huxleyi*, Journal of Plankton Research, 36, 316-325, 2013.

1352 Young, J. R. and Henriksen, K.: Biomineralization within vesicles: The calcite of coccoliths,
1353 Biomineralization, 54, 189-215, 2003.

1354 Young, J. R., Poulton, A. J., and Tyrrell, T.: Morphology of *Emiliana huxleyi* coccoliths on the
1355 northwestern European shelf – is there an influence of carbonate chemistry?, Biogeosciences, 11,
1356 4771-4782, 2014.

1357 Young, J. R. and Westbroek, P.: Genotypic variation in the coccolithophorid species *Emiliana huxleyi*,
1358 Marine Micropaleontology, 18, 5-23, 1991.

1359 Zondervan, I.: The effects of light, macronutrients, trace metals and CO₂ on the production of
1360 calcium carbonate and organic carbon in coccolithophores - A review, Deep-Sea Res. Part II-Top.
1361 Stud. Oceanogr., 54, 521-537, 2007.

1362 Zondervan, I., Rost, B., and Riebesell, U.: Effect of CO₂ concentration on the PIC/POC ratio in the
1363 coccolithophore *Emiliana huxleyi* grown under light-limiting conditions and different daylengths,
1364 *J. Exp. Mar. Biol. Ecol.*, 272, 55-70, 2002.
1365
1366

1367

1368

1369

1370

1371

1372

1373

1374

1375

1376

1377

1378

1379

1380

1381

1382

1383

1384

1385

1386

1387

1388

1389

1390

1391

1392

1393

1394

1395

1396

1397 **Tables**

1398 Table 1 – Entries in the database of coccolithophore metabolism

	Column content	Units/explanation
General information	Literature reference	-
	Coccolithophore species	Species name
	Coccolithophore strain	Strain name
	Experiment type	Batch or chemostat
	Optimal temperature of strain	°C
Experimental conditions	Duration light period	hours
	Duration dark period	hours
	Sampling time	hours from beginning of light period
	Irradiance	$\mu\text{mol photons m}^{-2} \text{ s}^{-1}$
	Temperature	°C
	Salinity	g/kg
	pCO ₂	μatm
	Dissolved inorganic carbon (DIC)	$\mu\text{mol kg}^{-1}$
	pH _T (total scale)	pH units
	Total alkalinity (TA)	$\mu\text{mol kg}^{-1}$
	Saturation state (calcite)	-
	Ca	mmol kg^{-1}
	Mg	mmol kg^{-1}
	NO ₃	$\mu\text{mol kg}^{-1}$
PO ₄	$\mu\text{mol kg}^{-1}$	
Experimental results	Organic C quota (POC)	pgC cell^{-1}
	Inorganic C quota (PIC)	pgC cell^{-1}
	Growth rate	day^{-1}
	Photosynthesis rate (RPh)	$\text{pgC cell}^{-1} \text{ day}^{-1}$
	Calcification rate (RCa)	$\text{pgC cell}^{-1} \text{ day}^{-1}$
	Coccosphere diameter	μm

1399

1400

1401

1402

1403

1404

1405

1406 Table 2 – Subgroups of experiments and the experimental conditions that define them

Group name	n	Irradiance	pCO ₂	TA	PO ₄	NO ₃	Fe	Ca
		μmol m ⁻² s ⁻¹	μatm	mmol kg ⁻¹	μmol kg ⁻¹	μmol kg ⁻¹	nmol kg ⁻¹	mmol kg ⁻¹
Optimum low pCO ₂	85	≥ 80	150 - 550	2.1 – 2.45	≥ 4	≥ 64	replete	9.3-10
Optimum High pCO ₂	87	≥ 80	551 - 1311	1.9 – 2.6	≥ 4	≥ 64	replete	9.3 – 11.1
Light-limited	30	< 80	140 – 850	2.0 – 2.56	≥ 4	≥ 64	replete	9.3-10
NO ₃ -limited	10	≥ 80	200-1200 ^a	2.3-4.5	≥ 4	limiting	replete	4-10
PO ₄ -limited	21	≥ 80	250-1200 ^a	1-4.5	limiting	≥ 64	replete	4-10.6
Fe-limited	1	180	?	~2.35	4	64	limiting	10

1407 ^aThe DIC system data presented in the literature does not lend itself to an accurate calculation
 1408 of DIC system.

1409

1410 Table 3 – Changes of cell and coccosphere (sphere) volume for given changes in
 1411 environmental conditions in culture experiments

Condition changed	Mean value of environment change	Average cell (sphere) volume change (μm ³)	Average % cell volume (sphere) change	Max cell volume (sphere) change (μm ³)	Max % cell volume (sphere) change
pCO ₂	+ 209 μatm	+8.6 (+6.7)	+14.4 (+5.2)	+23.5 (+51.9)	+34.6 (+36.6)
pCO ₂	+ 592 μatm	+12.6 (+10.3)	+27.3 (+12.8)	+63.4 (+131.8)	+214.2 (+185.6)
Irradiance	+ 193 μE m ⁻² s ⁻¹	+16.7 (+39.5)	+38.0 (+53.0)	+45.0 (+93.0)	+120 (+152.2)
NO ₃	Replete to limiting (~ 20 nM)	-14.0 (-33.0)	-22.2 (-22.5)	-26.3 (-80.0)	-33.1 (-36.8)
PO ₄	Replete to limiting (~ 0.3 nM)	+50.8 (+73.5)	+43.8 (+58.1)	+77.1 (+93.6)	+67.8 (+120.3)
Fe	Replete to limiting	-32.2	-69.9	-32.2	-69.9
Temperature	+ 7.6 °C (+5.8°C)	-25.8 (-40.4)	-27 (-18.8)	-75.1 (-144.0)	-68 (-57.8)

1412 Table 4 – Changes of cell and coccosphere (sphere) diameter for given changes in
 1413 environmental conditions in culture experiments

Condition changed	Mean value of environment change	Average cell (sphere) diameter change (μm^3)	Average % cell (sphere) diameter change	Max cell (sphere) diameter change (μm)	Max % cell (sphere) diameter change
pCO ₂	+ 209 μatm	+ 0.2 (+ 0.1)	+ 4.5 (+ 1.6)	+ 0.5 (+ 0.7)	+ 10.4 (+ 11.0)
pCO ₂	+ 592 μatm	+ 0.3 (+ 0.2)	+ 7.4 (+ 3.1)	+ 1.8 (+ 2.2)	+ 46.5 (+ 41.9)
Irradiance	+ 193 $\mu\text{E m}^{-2} \text{s}^{-1}$	+ 0.5 (+ 0.7)	+ 10.5 (+ 13.1)	+ 1.3 (+ 1.8)	+ 30.1 (+ 36.1)
NO ₃	Replete to limiting (~ 20 nM)	- 0.4 (- 0.5)	- 8.2 (- 8.3)	- 0.7 (- 1.1)	- 12.5 (- 14.2)
PO ₄	Replete to limiting (~ 0.3 nM)	+ 0.7 (+ 1.0)	+ 12.7 (+ 16.1)	+ 1.0 (+ 1.5)	+ 18.8 (+ 30.1)
Fe	Replete to limiting	-1.5	-33.3	-1.5	-33.3
Temperature	+ 7.6 °C (+5.8°C)	- 0.65 (-0.54)	-11.7 (-7.4)	-1.9 (-1.95)	-31.7 (-25)

1414

1415

1416

1417

1418

1419

1420

1421

1422

1423

1424

1425 **Figure captions**

1426 Figure 1 – Schematic representation of a coccolithophore cell surrounded by a shield of
1427 coccoliths. The coccolith bearing-cell is called the coccosphere (modified from Hendericks
1428 (2008)).

1429
1430 Figure 2 – Geometric model used to obtain cell and coccosphere geometry from measurements
1431 of the particulate organic carbon (POC) and particulate inorganic carbon (PIC) content per
1432 cell measured in culture experiments. Panels (a) and (c) show the relationship between POC
1433 and PIC and cell geometry (cell and coccosphere diameter) calculated with equation 7. Panels
1434 b) and d) show the relationship between the cell and coccosphere diameter calculated with
1435 equation 7 and that measured in culture experiments. Notes: panels (a) and (b) present data
1436 for *E. huxleyi*, panels (c) and (d) present data from the other coccolithophore species in the
1437 database. The filled black dots are the cell diameter, the empty red symbols are the
1438 coccosphere diameter and the empty blue symbols are the difference between the
1439 coccosphere and cell diameters.

1440
1441 Figure 3 – Allometric relationships between cell volume (equation 7) and photosynthesis rate
1442 (a,c) (equation 5), growth rate (b) (equation 3) and calcification rate (d) (equation 6). Notes:
1443 in panels (a) and (b) red dots are the experiments from the coccolithophore database carried
1444 out in optimum growth conditions and grey dots are published field measurements of
1445 metabolic rates for a large number of organisms (Marañón, 2008); in panels (c) and (d)
1446 symbols denote coccolithophore species (see legend) and all data refers to optimum growth
1447 conditions. The dotted lines are the linear regressions through the experimental
1448 coccolithophore data obtained in optimum growth conditions and the field data of Marañón
1449 (2008) (see table 2 for definition of optimum growth conditions).

1450
1451 Figure 4 – Effect of sub-optimum growth conditions on allometric relationships for
1452 coccolithophores. (a) rate of photosynthesis, (b) growth rate, (c) rate of calcification. Sub-
1453 optimum light and nutrient conditions result in cells having reduced metabolic rates
1454 compared to cells of equal size grown in optimal growth conditions (see table 2 for definition
1455 of growth conditions). The error bars apply only to a limited number of experiments (see
1456 text) and correspond to those experiments where the sampling time is not reported.

1457 Figure 5 – Changes in cell-size and metabolic rates of *E. huxleyi* cells (first two columns) and
1458 other coccolithophore species (last column) subject to an increase in pCO₂. Note: for *E.*
1459 *huxleyi* symbols denote optimum-low pCO₂ conditions (red circles), optimum-high pCO₂
1460 conditions (red dots), light-limited conditions (blue dots); for the other coccolithophore
1461 species symbols denote the species and all conditions are optimum, without distinction of
1462 pCO₂ range (see table 2 for definition of growth conditions).

1463

1464 Figure 6 - Changes in cell-size and metabolic rates of *E. huxleyi* cells subject to an increase in
1465 irradiance (starting from irradiance-limited conditions), an increase in temperature and a
1466 decrease in nutrients (starting from nutrient-replete conditions). The symbols represent the
1467 different growth conditions defined in table 2 except for iron for which there is only one
1468 datapoint.

1469

1470 Figure 7 – Geometry of Isochrysidales coccospheres along the BIOSOPE transect in the
1471 South-East Pacific ocean (Beaufort et al., 2008). (a) geographical location of the BIOSPE
1472 transect superimposed on the surface ocean chlorophyll concentration map obtained by
1473 satellite observations, (b) distribution of Isochrysidales coccosphere diameter in depth along
1474 the BIOSOPE transect determined by the SYRACO automated coccolith analyser system
1475 (Beaufort et al., 2008).

1476 Figure 8 – Comparison of the geometry (coccosphere diameter and volume) of *Isochrysidales*
1477 coccospheres from the BIOSOPE transect with the geometry of *E. huxleyi* coccospheres from
1478 laboratory culture experiments. Histograms in panels (a) and (b) compare BIOSPE field data
1479 (grey) with experimental data (red). Horizontal bar graphs in panels (a) and (b) show the
1480 average changes in coccosphere geometry observed in *E. huxleyi* culture experiments for
1481 given changes in pCO₂, irradiance, temperature, NO₃ and PO₄. (c) Box-whisker plots
1482 comparing environmental conditions at the BIOSOPE stations where *Isochrysidales*
1483 coccosphere geometry measurements were made (grey) with the range of environmental
1484 conditions imposed in laboratory culture experiments with *E. huxleyi* (red). Box-whisker
1485 plots show the minimum value, lower quartile, median, upper quartile and maximum value of
1486 a given environmental parameter. Note: size data for Fe-limitation is from one experiment in
1487 Schultz et al. (2007) and refers to cell-size (not coccosphere-size).

1488 Figure 9 – Simple physiological model of a dividing phytoplankton cell that reproduces the
1489 co-variation of metabolic rates and cell-size observed in coccolithophores. Notes: J_X –

1490 assimilation fluxes; J_{GX} – growth fluxes generated from the uptake of nutrient X ; J_{MATX} –
1491 maturation fluxes generated from the uptake of nutrient X ; J_G – total growth flux contributing
1492 to the buildup of structure (biomass) M_V ; P_R – total maturation flux contributing to the
1493 buildup of maturity E_H ; SU – synthesizing unit.

1494 Figure 10 – Evolution in time of modeled (a) maturity, (b) cell volume and (c) instantaneous
1495 growth rate of a cell undergoing ten successive cycles of growth and division. Notes: the
1496 horizontal dashed line in (a) represents the threshold value of accumulated maturity in the
1497 cell at which cell division takes place; the horizontal dashed line in (b) is the average cell
1498 volume when cell cycles attain steady state, the horizontal dashed line in (c) is the average
1499 instantaneous growth rate when cell cycles attain steady state and is numerically equivalent to
1500 the growth rate calculated from the generation time (vertical dashed lines) via equation 22 – it
1501 is conceptually equivalent to the growth rate measured from cell-counts in culture
1502 experiments.

1503 Figure 11 – Effect of changing nitrate and phosphate concentrations on modeled cell volume
1504 and growth rate (a, c, d, e and f) and on the maturation flux P_R and the ratio of the growth to
1505 maturation fluxes P_G/P_R (b). Notes: the data points in (d) and (f) correspond to the shifts in
1506 cell-size and growth rate observed in laboratory cultures with *E. huxleyi* subject to a decrease
1507 in nitrate (d) and phosphate (f) concentrations.

1508

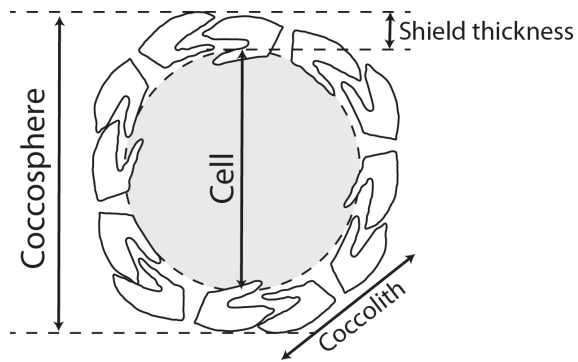


Figure 1

1509

1510

1511

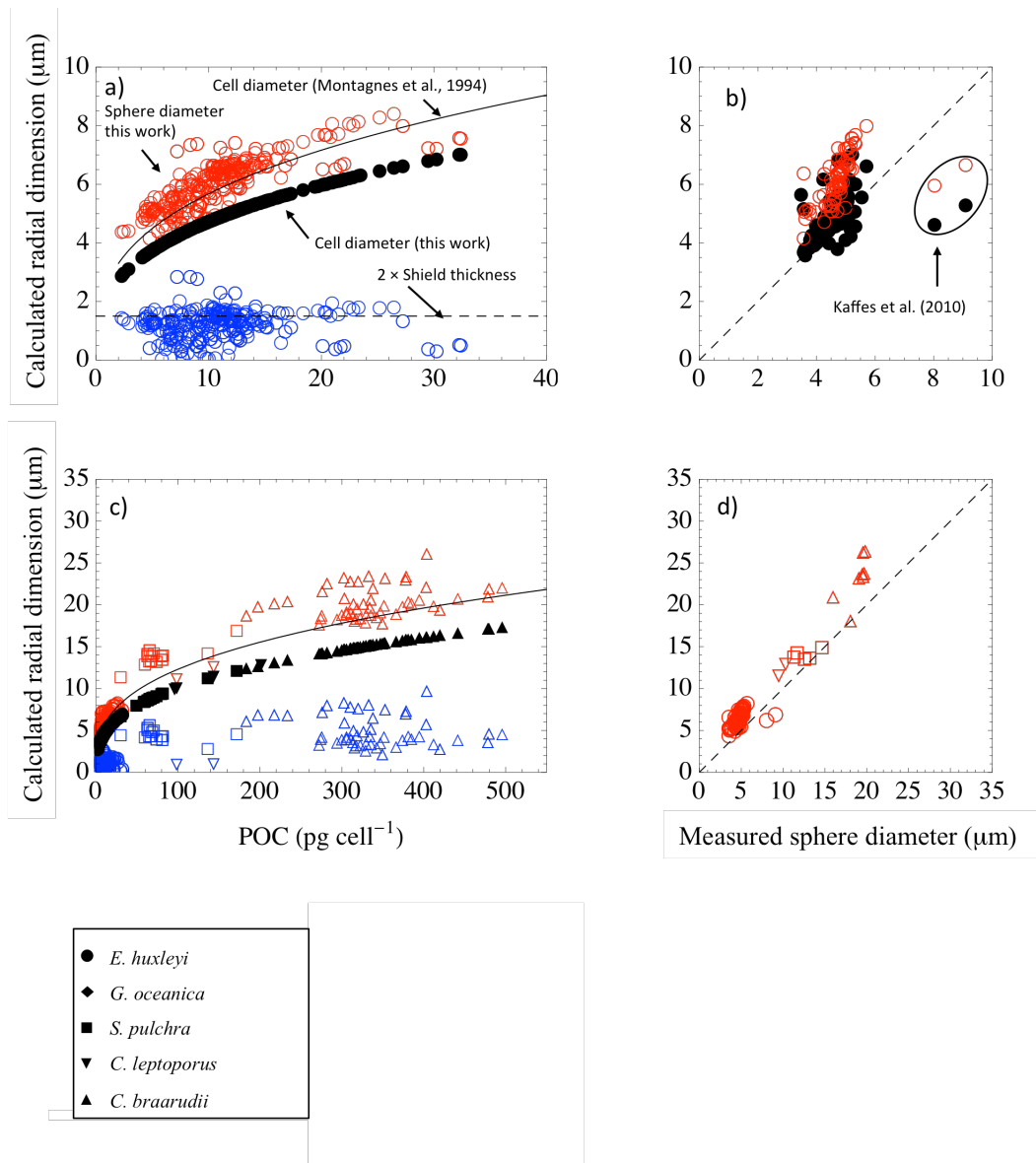


Figure 2

1512
 1513
 1514
 1515
 1516
 1517
 1518
 1519
 1520
 1521

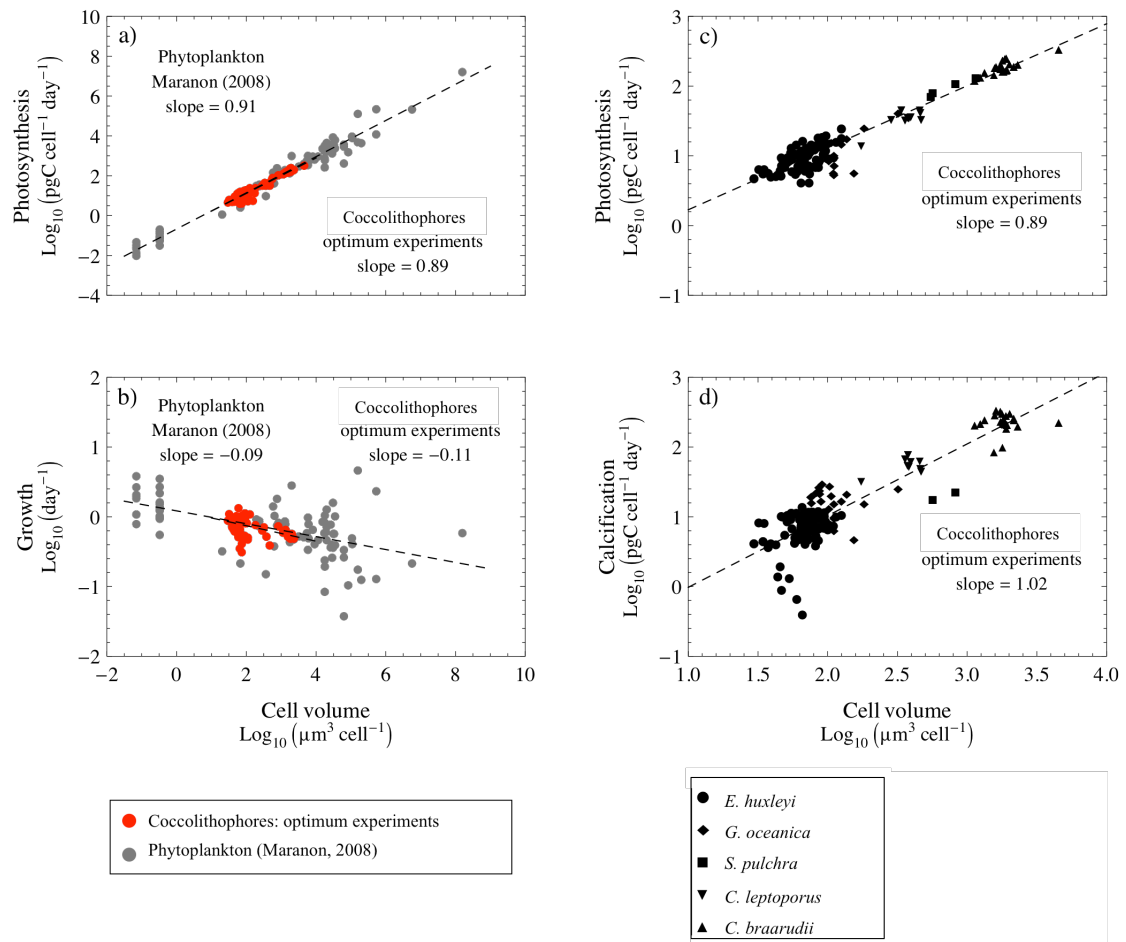


Figure 3

1522
 1523
 1524
 1525
 1526
 1527
 1528
 1529
 1530

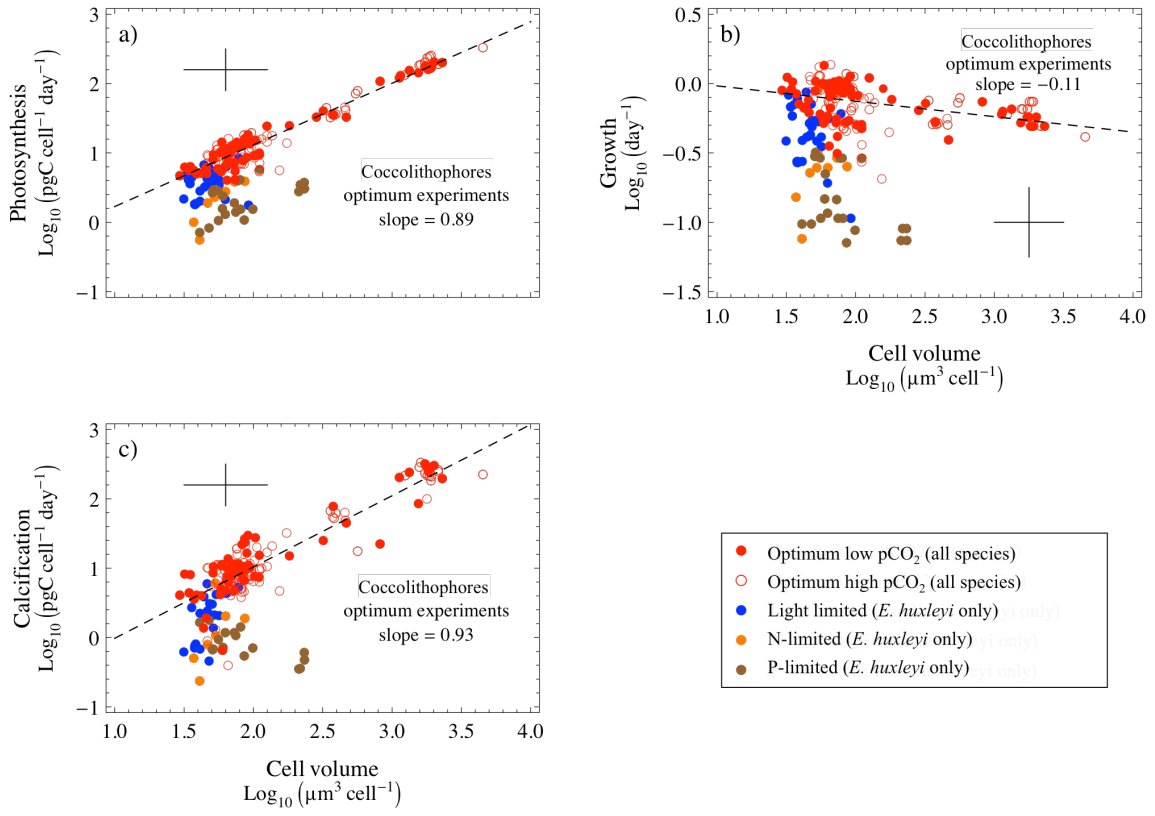


Figure 4

1531

1532

1533

1534

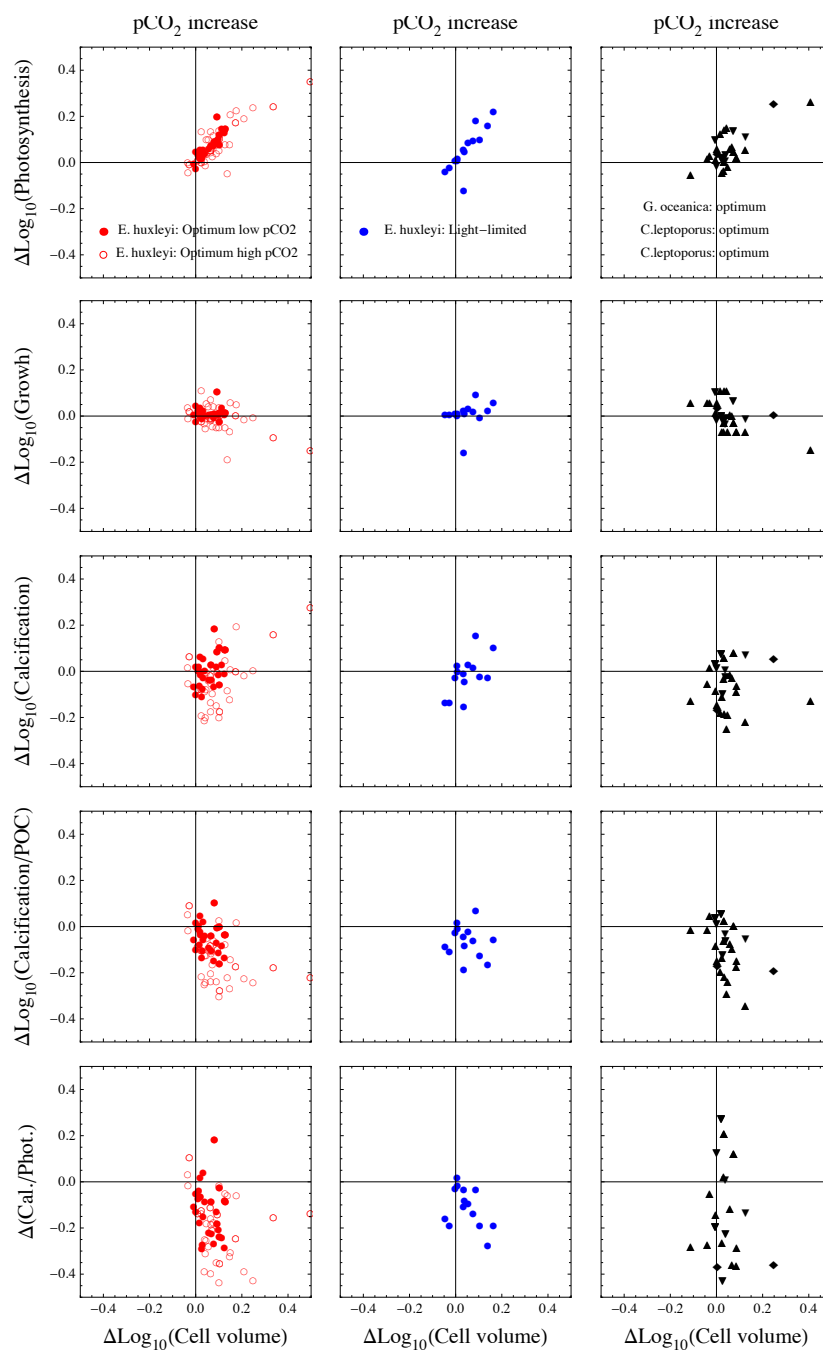


Figure 5

1535

1536

1537

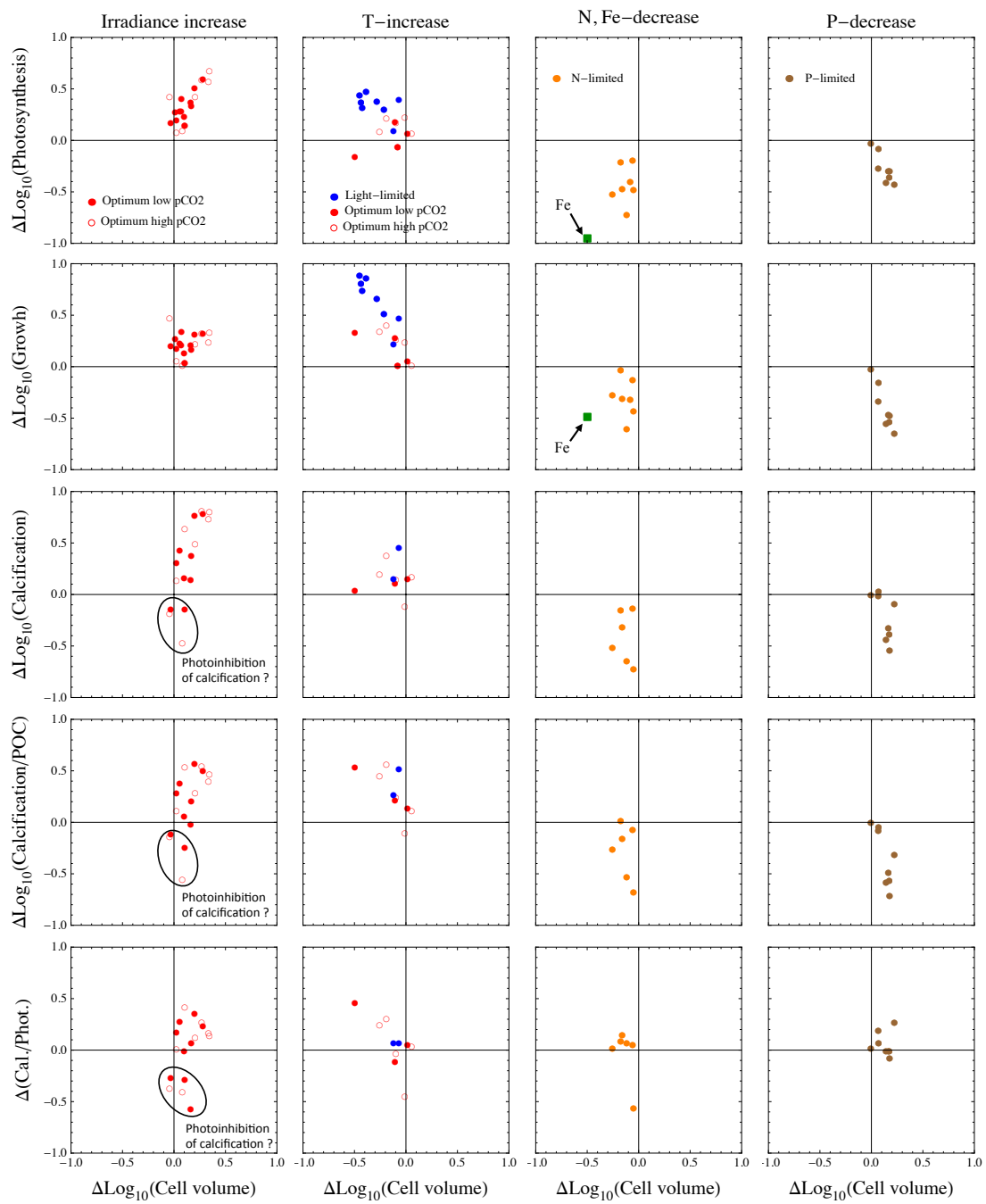


Figure 6

1538
 1539
 1540

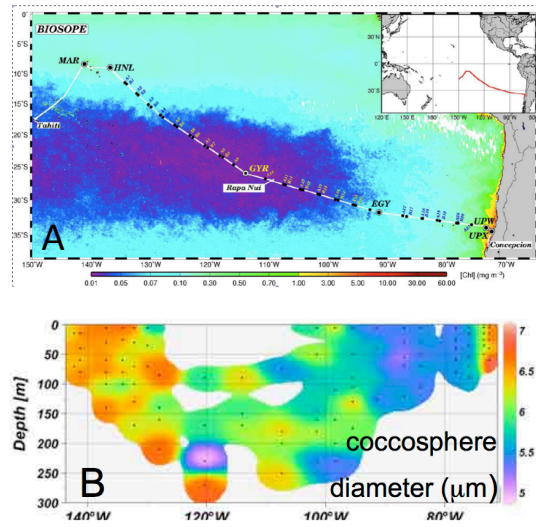


Figure 7

1541

1542

1543

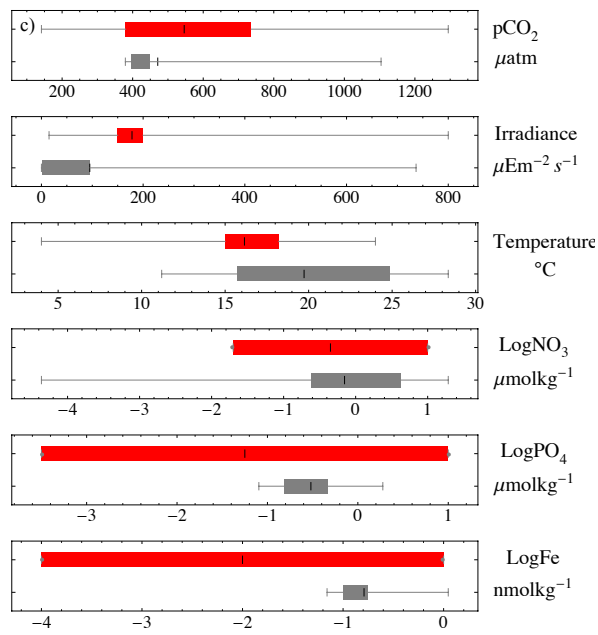
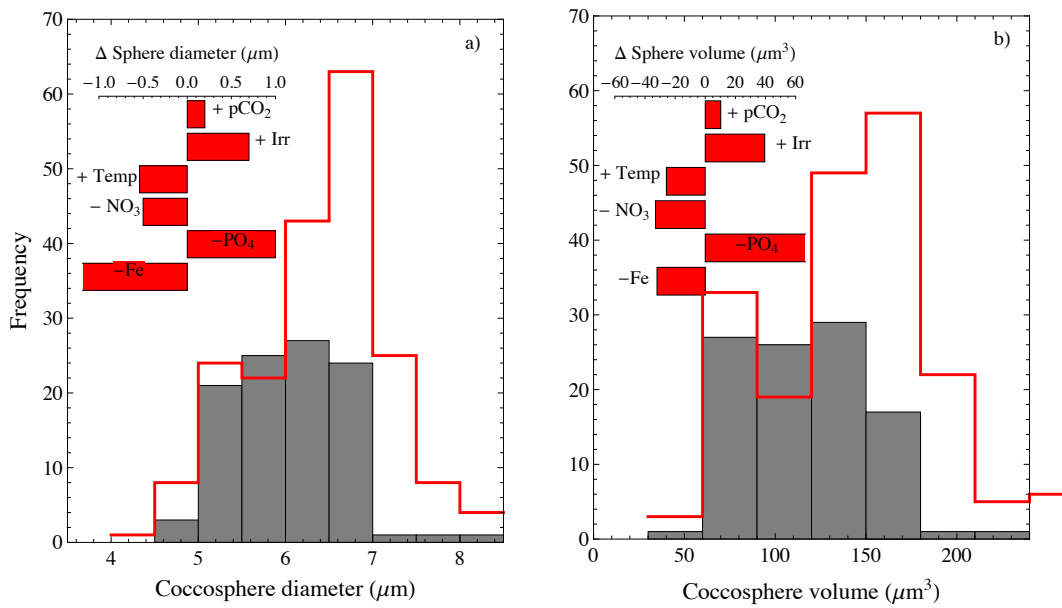


Figure 8

1544

1545

1546

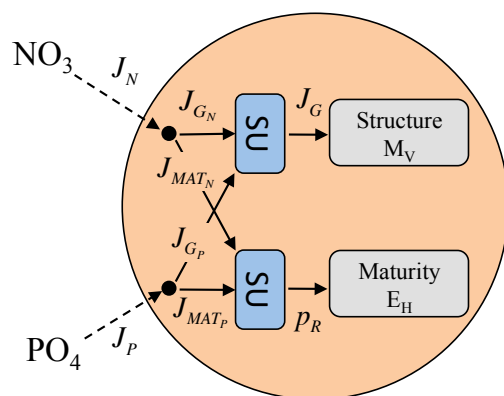


Figure 9

1547

1548

1549

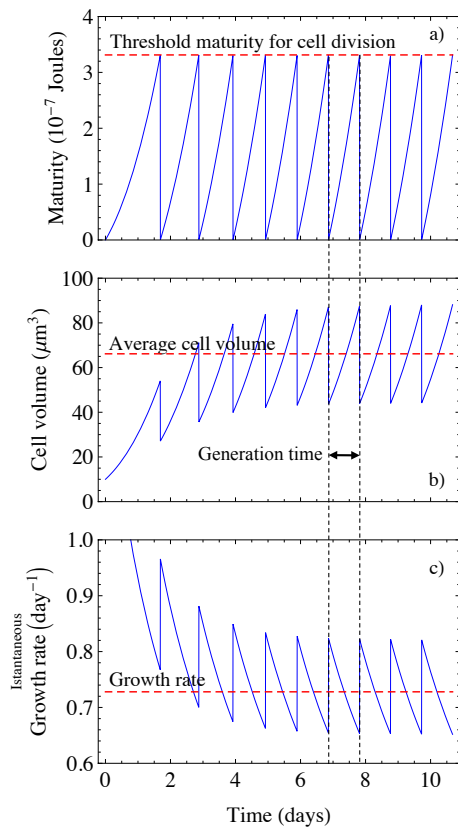


Figure 10

1550

1551

1552

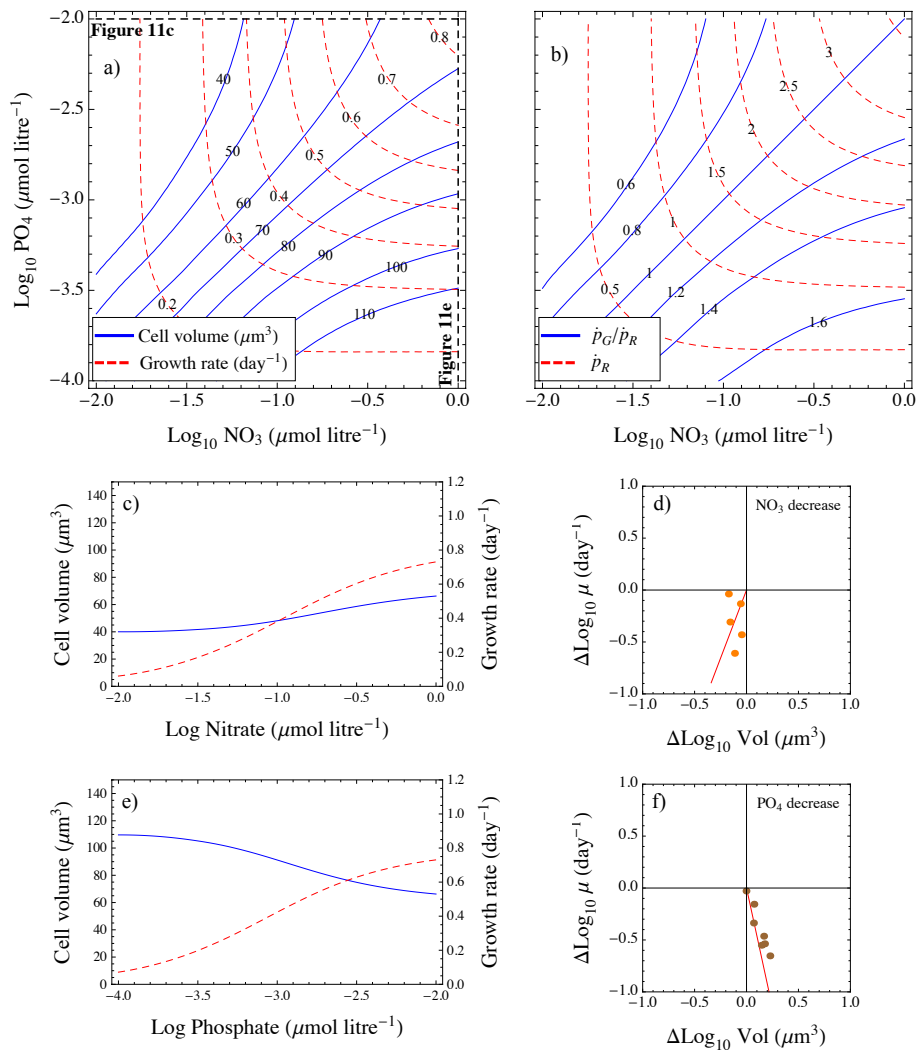


Figure 11